SAND2013-6879J

Role of Microstructure and Doping on the Mechanical Properties of Polysilicon Thin Films

Sivakumar Yagnamurthy, Brad L. Boyce and Ioannis Chasiotis

***Abstract*—The role of grain size and doping on the mechanical reliability of 1-µm thick polysilicon films was investigated, in terms of flaw dependent mechanical strength, and the mode I critical stress intensity factor, K_{IC}. The films were comprised of either columnar (grain size 285 nm) or laminated (grain size 125 nm) polysilicon doped with different concentrations of Phosphorus. Columnar polysilicon typically had 1-2 grains across the thickness of the film, whereas laminated polysilicon films had up to ten grains across the film thickness. The average strengths of undoped columnar and laminated polysilicon were 1.28±0.06 GPa and 2.28±0.15 GPa, respectively. Heavy doping impacted the strength of the former (0.99±0.05 GPa) due to the formation of large sidewall defects, which were dependent on the concentration of Phosphorus which, however, had no effect on laminated polysilicon. On grounds of Weibull statistics, the results of the present experiments predicted quite accurately experimental data from tensile bars that were 180 times smaller by volume. Also, the study examined the remediating role of ion milling to remove surface defects and improve strength. The fracture strength of columnar polysilicon increased by 70-100%, approaching the tensile strength of laminated polysilicon that underwent a similar ion milling process. Measurements of fracture toughness, K_{IC}, were used to evaluate the effect of doping on the intrinsic fracture resistance of the two types of polysilicon. On average, the K_{IC} of columnar polysilicon was higher than that of laminated polysilicon, but the latter demonstrated smaller variability in K_{IC}, which was owed to the averaging effect of its laminated structure. Crack arrest and re-initiation was possible for columnar polysilicon subjected to a ramp load: the crack initiated at K_{IC} = 0.82 MPa√m, arrested in an adjacent grain, and finally re-initiated at K_{IC} = 1.1 MPa√m followed by catastrophic crack growth.**

***Index Terms*—Critical stress intensity factor, microstructure, grain size, doping, size effects**

This work was supported by the Air Force Office of Scientific Research (AFOSR) through Grant FA9550-09-1-0535 with Dr. B.L. Lee as the program manager.

S. Yagnamurthy and I. Chasiotis are with Department of Aerospace Engineering, University of Illinois, Urbana-Champaign, IL 61801 USA (e-mail: syagnam2@illinois.edu; chasioti@illinois.edu)

B.L. Boyce is with Sandia National Laboratories, P.O. Box 5800, MS0889, Albuquerque, NM 87185, USA (e-mail: blboyce@sandia.gov). BLB was supported by the Department of Energy, Office of Basic Energy Sciences. Sandia National Laboratories is a multi-program laboratory managed and operated by Sandia Corporation, a wholly owned subsidiary of Lockheed Martin Corporation, for the U.S. Department of Energy's National Nuclear Security Administration under contract DE-AC04-94AL85000.

I. Introduction

Polycrystalline silicon ('polysilicon') has been the most common material for surface micromachined Microelectromechanical Systems (MEMS) because of its advantageous electrical and mechanical properties as well as the mature and versatile fabrication processes for intricately shaped devices [1]. Surface micromachined MEMS perform most reliably as two-dimensional suspended devices comprised of slender beams and flexures to allow for large in-plane displacements under relatively low forces. However, in order to reach the desired motion, slender components can be subject to large stresses that often exceed 1 GPa. The brittle nature of polysilicon MEMS presents the advantage of dimensional stability but raises the concern of catastrophic fracture due to voids, crevices or micro-cracks on the surface or in the stressed volume of a device [2]. Prior research has shown the potential of increasing the mechanical strength of small polysilicon parts to ~3.5 GPa [3,4], which, however, is still far from the experimental reports of near theoretical strength for defect free single crystal silicon beams. For instance, the intrinsic strength of single crystal silicon has been shown to be of the order of 1-20 GPa [5], which is by far higher than the tensile strength of polycrystalline silicon reported in the range of 1-5 GPa [3,6-10], and depends on specimen size consistently with expectations for brittle materials [2,8,11]. Past research has shown that deposition, Reactive Ion Etching (RIE), doping and sacrificial etching influence in different degrees the specimen porosity, surface and sidewall roughness [12], which are among the primary forms of catastrophic flaws. Furthermore in the presence of metallization layers, e.g. Au, it has been shown that the mechanical strength is strongly affected by the extent and nature of the sacrificial etching method [4,13,14]. Other microstructures, such as laminated polysilicon or amorphous silicon, have been shown to resist failure until 9.7 GPa compared to 5 GPa for that of columnar polysilicon [15]. The difference in fracture strength has been attributed to fewer process related flaws present on the free surface of polysilicon films. At the other extreme, Tsuchiya *et al* [16] reported the strength of amorphous silicon to be lesser than that of polysilicon, potentially due to the presence of 0.4% atomic hydrogen and large defects in amorphous silicon. The strength of polysilicon also depends on the annealing temperature, which, in turn, dictates the grain size. While the grain size does not directly impact the fracture strength, the size of defects formed for larger grain sizes are bigger, thus resulting in lower strength compared to small grain polysilicon.

Contrary to metals, however, there is no mechanistic correlation between grain size and strength for perfectly brittle materials. Therefore, the origins of lower strength for large grain polysilicon should be sought in the side effects of the fabrication methods, e.g. prolonged annealing at high temperature and high Phosphorous (P) doping, used to grow large grain polysilicon [17].

The resistance of the material itself to fracture is quantified independently of the flaw size via fracture experiments with pre-fabricated cracks of well-known geometry and dimensions. A reference for the expected values for the critical stress intensity factor, K_{IC}, is provided by single crystal silicon data [18-21], which can be as low as 0.82 MPa√m for (111) planes [19], and as high as 1.22 MPa√m according to [18]. More specifically, the K_{IC} values for single crystal silicon (100), (110) and (111) planes have been reported as 0.95 MPa√m, 0.90 MPa√m and 0.83 MPa√m, respectively [19]. The values of K_{IC} for polysilicon films have been reported by several groups [22,23], with the most recent reports providing distributions of values in the range of 0.8-1.2 MPa√m [24,25], where the variation in values was attributed to local material anisotropy near the crack tip and grain heterogeneity. A direct consequence of this distribution of values for the effective critical stress intensity factor, $K_{IC,eff}$, which incorporates the effect of local variations in microstructure, is that cracks could arrest as long as $K_{IC,eff}$ is less than 1.2 MPa√m [24], thus leading to R-curve behavior. In a computational cohesive-zone analysis, Foulk *et al* [26,27] demonstrated that the grain shape, crystal lattice orientation and grain boundary (GB) strength can increase $K_{IC,eff}$ by local crack tip deflection. Thus, modification of the grain structure and potentially the energy landscape between grains and GBs could affect the resistance to crack initiation. The energy landscape could be modified by dopants such as P that are known to segregate to GBs and promote grain growth [17]. However, the effect of P doping on toughening and strengthening is inconclusive [28,29]. For instance Zeng *et al* [28] reported a 3% increase in the critical stress intensity factor of silicon that is heavily P doped, whereas Swadener *et al* [29] reported an equally insignificant effect. If GBs and triple junction points influence the crack path and hence $K_{IC,eff}$, influencing the cohesive strength of GBs via doping may provide an additional control of crack initiation and arrest. Phosphorous doping also has indirect consequences to grain growth during annealing [17,30-32], which, in turn, may affect the material failure strength.

This work aims at addressing the convoluted effect of doping and grain size on the tensile strength and the $K_{IC,eff}$ of polysilicon fabricated in an experimental run at the Sandia National Laboratories. The mechanical properties of polysilicon manufactured by the regular SUMMiT V^{TM} process by the Sandia National Laboratories have been reported before by Chasiotis and Knauss [3] and Boyce *et al* [8], who identified the specimen sidewalls as the location of the flaws controlling failure. More recently, a new microstructure has been explored for the same process, in which a polysilicon structural layer has been substituted by a laminated structure that reduces the grain size. The data presented here sheds light on the critical flaw formation and the role of doping in the intrinsic mechanical behavior, as manifested by the material fracture toughness, and the mechanical strength that reflects the content and type of flaws. A first report on the two types of polysilicon films considered in this study by Boyce *et al* [33] presented a 60-90% increase in strength for laminated compared to columnar polysilicon. This work addresses several ensuing questions, among them the scalability of polysilicon strength to much larger dimensions than previously studied, and the convergence of the mechanical strength of the two types of films, once the critical flaws in columnar polysilicon are eliminated. Furthermore, a thorough fracture mechanics analysis coupled with a critical evaluation of edge and surface flaws is used to make mechanical strength predictions based on simple defect analysis. Finally, experiments with prefabricated sharp cracks are employed to elucidate the role of grain homogeneity and dopant content on the local fracture behavior of the two types of polysilicon.

II. Experimental methods

A. Materials and Fabrication

Two types of 1-μm thick polysilicon specimens were fabricated by a custom polysilicon fabrication run at Sandia National Laboratories: Specimens with grain size of 285 nm (film in-plane dimensions), which is smaller than the standard SUMMiT V^{TM} microfabrication process [34,35], and specimens with laminated structure and grain size of 125 nm [33]. The grain structure of the former polysilicon was fairly columnar and henceforth we refer to it as "columnar polysilicon" whereas the latter polysilicon with finer grain size will be referred to as "laminated polysilicon". The initial processing steps were identical for both microstructures. First, a 0.63 μm thick oxide layer was thermally grown on the silicon wafer followed by 0.8 μm thick low–stress nitride layer using LPCVD. These blanket films act as electric insulating layers between the wafer and operating MEMS structures. A 0.3-μm thick LPCVD polysilicon (Poly0) layer was deposited on top of the nitride layer as a ground layer. A 2 μm thick sacrificial oxide layer (SacOx1) of either phosphosilicate glass (PSG) with 0.5% or 2% P or undoped silane glass was then deposited and patterned. Subsequently, a 1-μm thick columnar polysilicon layer (Poly1) was deposited in a furnace at 580 °C. The laminated polysilicon was fabricated by depositing 10 alternate layers of 100 nm thick amorphous and polycrystalline silicon resulting in a 1 μm thick composite. A second sacrificial oxide layer (SacOx2) was deposited on top of Poly1 and was chemo-mechanically planarized to a thickness of 2 μm. All wafers were then annealed in N_2 environment for 1hr at 1050 °C to allow for diffusion of P. In the case of laminated polysilicon, the amorphous silicon became polycrystalline during annealing and resulted in the laminated structure shown in Fig. 1(c). SEM images of the cross-section of columnar and laminated polysilicon are shown in Fig.s 1(b) and 1(c), respectively. The top surface of columnar polysilicon contained abnormal grains measuring more than 500 nm and in some extreme cases these grains measured as much as 500 × 1000 nm. Chemical analysis of these abnormal grains by Energy Dispersive Spectroscopy (EDS) indicated the presence of silicon atoms only. Hence, these abnormal silicon grains are possibly the result of recrystallization during annealing at high temperature.

Notably, the surface topography of laminated polysilicon was very uniform compared to columnar polysilicon.

The uniaxial tension specimens were 100 μm wide with a gage length of 1,000 μm, shown in Fig. 1(a). For the purpose of fracture experiments, sharp cracks were introduced into the specimen gauge section by a microhardness indenter as described in [24]. In this method, an indent is generated to the sacrificial oxide layer alongside the tensile specimen and one of the edge cracks extending from the corners of the indent grows into the polysilicon specimen [24,25]. SEM and AFM images of the cracks and their tips were obtained for each specimen to measure the crack length and record the precise location of the crack tip with respect to the grain structure. Fig. 2 shows the SEM and AFM images of a crack and its tip, respectively, in undoped columnar and laminated polysilicon. After indentation, the films were etched in 49% HF to obtain freestanding specimens for fracture experiments.

B. Fracture Toughness and Tensile Strength Experiments

Use

An apparatus for microscale uniaxial tension experiments, described in previous works [36], was employed for the strength and fracture toughness measurements. The experimental apparatus consisted of a PZT actuator for loading the specimen in tension and a 50g capacity loadcell to measure the applied force to the specimen. The PZT actuator and loadcell were mounted on linear and rotational micro-positioners to control specimen alignment to apply uniaxial tension. All experiments were conducted at the strain rate of 6×10^{-4} s^{-1}. The K_{IC} from the edge cracked specimens was calculated using the linear elastic fracture mechanics (LEFM) solution [37]:

$$K_{Ic} = \sigma_{\infty} Y \sqrt{\pi a} \tag{1}$$

where σ_{∞} is far field stress, a is crack length, and Y is shape function calculated by

$$Y = 1.122 - 0.231\left(\frac{a}{w}\right) + 10.55\left(\frac{a}{w}\right)^2 - 21.71\left(\frac{a}{w}\right)^3 + 30.382\left(\frac{a}{w}\right)^4 + HOT \tag{2}$$

where w is specimen width. The specimen thickness was measured by an SEM, and was in good agreement with the nominal values calculated using the deposition rate and times.
The Young's modulus and fracture strength were computed from the results of uniform tension experiments. During an experiment, pictures of specimen surface were recorded using an optical microscope at 200× magnification and a two-dimension digital image correlation (DIC) analysis was performed to compute the full-field strain, which was plotted together with the measured stress values.

III. RESULTS

The calculated K_{IC}, fracture strength and Young's modulus for columnar and laminated polysilicon thin films doped with different concentrations of P are given in Table 1 and plotted in Fig. 3 and 4. A minimum of 15 specimens were tested for each specimen kind. The K_{IC} from all the polysilicon thin films was in the range of 0.82-1.27 MPa√m which agrees with the range of K_{IC} values for bulk silicon [18-20] and the K_{IC} for polysilicon fabricated by a different process (MUMPS) previously reported by this group [24,25]. The average K_{IC} varied slightly with grain structure and with doping level. Specifically, the K_{IC} values for columnar polysilicon were in the range of 0.88–1.2 MPa√m and were slightly higher than those of laminated polysilicon that were in the range of 0.85-1.08 MPa√m, averaging 0.95±0.08 MPa√m and 0.99±0.05 MPa√m, respectively. Notably, there was substantial scatter in the values of K_{IC} for specimens belonging to the same die, by as much as 40%. This scatter was actually larger for columnar polysilicon doped with 0.5% and 2% PSG compared to laminated polysilicon.

The fracture strength results for as-fabricated specimens are given in Fig. 4. The average strength of columnar polysilicon was 1.30±0.09 GPa which is 44% lower than that of the laminated polysilicon that was measured as 2.32±0.15 GPa. Notably, while the strength of columnar polysilicon doped with 2% PSG dropped to 0.95±0.07 GPa, i.e. 23% lower than the undoped material, the strength of columnar polysilicon doped with 0.5% PSG measured was same as that of undoped polysilicon. However, the strength of laminated polysilicon did not change significantly with doping. Unlike the fracture strength, the Young's modulus of polysilicon was independent of grain structure and doping level as shown in Table 1.

Due to the brittle nature of polysilicon and its high strength, the specimens shattered upon failure and hence, post fracture analysis of the cross sections could not be carried out. The statistical dependence of strength on specimen size was quantified by using the Weibull distribution function [38]. The cumulative probability function for the three-parameter Weibull distribution for uniform tension is given by

$$P = 1 - \exp\left(-\left(\frac{\sigma - \sigma_u}{\sigma_c - \sigma_u}\right)^m\right) \tag{3}$$

where σ_u is the threshold stress below which no failure is expected to occur, σ_c is the characteristic stress, and m is the Weibull modulus. The probability of failure for a specimen at each stress level was computed using the estimator

$$P_n = \frac{n - 0.5}{N} \tag{4}$$

where P_n is the probability of failure of n^{th} specimen and N is the total number of specimens tested. The cumulative distribution function was rewritten as

$$\ln\left(-\left(1-P\right)\right) = m\ln\left(\frac{\sigma-\sigma_u}{\sigma_c-\sigma_u}\right) \quad (5)$$

to obtain m, σ_c and σ_u from the cumulative probability distribution shown in Fig. 5. The m, σ_c and σ_u calculated for both the two and three parameter Weibull distributions are provided in Table 2.

The characteristic strengths for each type of specimen calculated from the Weibull analysis using the two and the three parameter analysis were practically the same. The Weibull modulus of columnar polysilicon was 50% larger than that of laminated polysilicon indicating that the defects causing failure of columnar polysilicon are of very consistent size and location. This consistency in the value of Weibull modulus of columnar polysilicon implies that the relevant catastrophic flaws were potentially introduced during post-processing such as Reactive Ion Etching (RIE) or annealing rather than being random flaws owed to the material grain structure developed during deposition. The latter are commonly surface roughness related flaws and result in Weibull moduli of the order of 10 or lower.

IV. Discussion

A. Effect of Grain Structure and Doping on Tensile Strength

The mechanical strength is the defining metric for MEMS reliability and design. Microstructurally speaking, the large (80%) difference in strength between laminated and columnar microstructures is not due to substantial differences in fracture toughness for the two microstructures, since their toughness values were nearly identical. Local fracture parameters such as K_{IC} are important in understanding microstructural effects on intrinsic bond fracture because they are derived from a well-controlled defect geometry. In terms of mechanical strength, the Weibull strengths of columnar and laminated polysilicon specimens were in the range of 1-1.3 GPa and 2.3-2.5 GPa, respectively. For the same custom polysilicon films, Boyce *et al* [33] reported that characteristic strengths of columnar and laminated polysilicon as 1.76 GPa and 2.80 GPa, respectively, showing that laminated is substantially stronger than columnar polysilicon. The strength values reported in that previous work are 15-35% higher than that reported here for 180 times smaller (~150×3.74×1 μm^3) specimen sizes by volume (7 times smaller by sidewall surface area). Table 3 compares the characteristic strength and the Weibull modulus of polysilicon measured in this work with those reported in [33]. The measured strength of brittle materials depends on the size of the specimens tested. Increasing the specimen size enhances the probability of larger critical flaws present in a specimen and reduces the measured strength. The characteristic strength of both columnar and laminated polysilicon decreased with increasing specimen size, as expected. Meanwhile, the Weibull modulus of columnar polysilicon increased by 40-90% indicating that the critical flaws were more evenly distributed in larger specimens (the larger specimen volume included all types of flaws that resulted in failure), it did not show a particular trend for laminated polysilicon.

The consistency of the Weibull parameters extracted from the two specimen sizes in this work and in [33] was evaluated using the Weibull statistics:

$$\sigma_{c,1} = \sigma_{c,2}\left(\frac{V_2}{V_1}\right)^{\frac{1}{m_2}} \quad (6)$$

$$\sigma_{c,1} = \sigma_{c,2}\left(\frac{A_2}{A_1}\right)^{\frac{1}{m_2}} \quad (7)$$

The characteristic strength of large specimens was estimated using the Weibull parameters measured from small specimens and *vice versa*, assuming that the critical flaws are distributed in (a) the sidewall surface area, and (b) the specimen top surface area. Given that the specimen thickness was 1 μm for both the small and the large specimens, the analysis for the sidewall surface area is equivalent to a specimen length or a specimen edge analysis, whereas the analysis for the specimen top surface area is equivalent to an analysis of volumetric flaws. On the other hand, due to the constant film thickness, this analysis cannot distinguish between volumetric critical flaws and top surface area critical flaws. The bar charts in Fig. 6(a,b) provide support that the Weibull size effect is governed by critical defects residing on or along the specimen sidewall surface, as the σ_c of large specimens can be closely predicted from experimental data from small specimens and *vice versa*. An analysis using the specimen top surface area did not result in as good agreement between the two data sets as shown in Fig. 6(c,d).

The Weibull-based analysis is further corroborated by Atomic Force (AFM) and Scanning Electron Microscopy (SEM) images of the specimen top and sidewall surfaces of columnar and laminated polysilicon specimens. Based on AFM images, the top RMS surface, average peak-to-valley, and maximum peak-to-valley roughness of laminated polysilicon was nearly same, 12%, and 26% lower than columnar polysilicon. Such variations in average roughness does not entirely explain the large difference in tensile strength; instead one must look for individual defects on all specimen surfaces such as those shown in Fig. 7(a,b) for columnar polysilicon. Such large flaws appear to have originated in post processing, whereas defects formed during deposition process are expected to be smaller in size. The sidewall flaws were all located at the top edge of specimen and were always associated with severe GB grooving of large grains. Notably, GB grooving occurred by GB pitting, which, although it was present on the entire specimen surface of 2% PSG doped columnar polysilicon, Fig. 8(a), it was most detrimental at the specimen sidewalls, or at the top edge of the specimen. On the contrary, the sidewall surface and the top surface of laminated polysilicon were smooth as shown in Fig. 7(c) without evident GB grooves.

GB grooving was dramatically more pronounced for P doped columnar polysilicon as shown in Fig. 8(a) and 9. Contrary to the small effect on K_{IC}, heavy doping (2% PSG)

had significant impact on the fracture strength of the columnar polysilicon, reducing it by 30% compared to undoped polysilicon. On the contrary, lightly doped columnar polysilicon with 0.5% PSG exhibited the same fracture strength as that of undoped, which provides a path to safe doping. Heavily doped polysilicon was characterized by deep crevices and GB grooves at the top edge of the sidewalls as shown in Fig. 8(a), notably larger than any ridges owed to RIE. These crevices were much less pronounced on lightly doped and undoped specimens shown in Fig. 8(b,c), which had virtually identical sidewall morphology and hence fracture strength.

While defects in a material can originate because of various processes, such as CVD deposition, RIE, doping, and annealing, the defects shown in Fig. 7(a,b), 8(a), and 9 are not polysilicon growth deposition related since they are found only at the sidewalls. Similarly, they cannot be RIE related since doped and undoped columnar polysilicon underwent the same RIE process prior to annealing and no such defects were observed in undoped films. While it has been shown that prolonged etching of polysilicon in 49% HF acid causes porosity and micro-cracks in presence of metallization layer, this does not entirely explain the formation of such deep crevices only at the sidewalls. The specimens etched in 49% HF for very short times that were sufficient to etch only the top 2-μm sacrificial oxide still contained sidewall defects similar to those shown in Fig. 8(a), which implies that sacrificial etching was not responsible for those serious crevices.

Instead, the large sidewall edge defects could have originated in the P diffusion and annealing processes. According to Robertson [39], GB grooving occurs in polysilicon at high temperatures due to self-diffusion of silicon at GBs into adjacent grains. It has been shown that very minimal grain growth occurs in undoped polysilicon during annealing over 1000º C and this increase with the addition of P dopants [17]. While Wada *et al* [40] saw a limited grain growth in polysilicon with P concentrations of 2.5×10^{20} atoms/cm^3, a remarkable increase in grain growth occurred for polysilicon doped with 7.5×10^{20} P atoms/cm^3. A critical concentration of P in polysilicon for enhanced grain growth is thus ~4×10^{20} atoms/cm^3. In the present study, the concentration of P in 0.5% PSG and 2% PSG was 2.25×10^{20} atoms/cm^3 and 9×10^{20} atoms/cm^3, respectively. During annealing of highly doped columnar polysilicon (2% PSG), high P diffused into polysilicon GBs, especially at GBs near the sidewalls due to diffusion from top and lateral surfaces. At annealing temperatures in the range of 1000-1100º C, secondary recrystallization is expected for heavily doped polysilicon where larger grains grow at the expense of smaller ones. Moreover, phosphosilicate glass with high concentrations of P reflows at temperatures over 900º C. During annealing, the phosphorus pentoxide (P_2O_5) in PSG undergoes a reduction reaction with Si to form SiO_2 and P [41]. It is therefore likely that a combination of secondary grain growth and reduction reaction of P_2O_5 resulted in increased formation of SiO_2 at GBs. When the sacrificial oxide layers are etched in 49% HF acid, the newly formed SiO_2 at GBs is etched away resulting in the pores seen at GBs in Fig. 9. Due to the high P content at the GBs near sidewalls, the formation of pores in this region was enhanced. Often, these pores coalesced around a grain near a sidewall, Fig. 9, to separate the grain from the film, thus causing deep crevices, such as that in Fig. 7(a). The presence of pores and deep crevices was more pronounced in columnar polysilicon doped with 2% PSG, whereas such large defects were not found in undoped and 0.5% PSG columnar polysilicon. Thus, the presence of P beyond a critical concentration exacerbates defect formation during annealing. On the other hand, no such defects were observed on the surface of 2% PSG doped laminated polysilicon, whose fracture strength was 2.46±0.22 GPa and was unaffected by doping: presumably the large GB network in the smaller grain laminated polysilicon provided a more even distribution of P near the top surface. On the other hand, the laminated structure generated small equiaxed grains which limited the depth of each grain and the formation of deep diffusion zones for P, which was the case for columnar polysilicon. To confirm this potential explanation, a much more detailed analytic transmission electron microscopy or atom probe study is needed to quantify the precise spatial variation of P content before and after annealing for these different microstructures.

B. Effect of Grain Structure and Doping on Local Fracture Initiation

The role of GBs and P doping in the local fracture behavior of polysilicon, can be evaluated by fracture mechanics measurements which can indicate whether (a) GBs increase or decrease the fracture propensity, and (b) whether high P concentration changes the local energy release rate upon fracture initiation due to a flaw.

The values of K_{IC} for undoped polysilicon films were in agreement with those reported by this group before for a different source of polysilicon MEMS from the MUMPs process, namely in the range of 0.8-1.2 MPa√m [24,25]. Due to the polycrystalline nature, the location of the initial crack tip generated in the specimens could be either inside a grain or at a GB. In [24,25] it was shown that the presence of GBs increases the effective K_{IC} of polysilicon. However, three dimensional effects can overshadow such conclusions stemming from 2D material considerations. For instance, Fig. 10(a,b) show AFM images of two different specimens belonging to the same die but exhibiting K_{IC} values of 0.88 MPa√m and 1.03 MPa√m, with the crack tip residing at a GB and inside a grain, but near a triple junction point, respectively. This variability in the measured effective K_{IC} was more pronounced for undoped columnar than for laminated polysilicon, as shown in Fig. 3. This was due to the random distribution of columnar grains with different orientation where K_{IC} was mostly dependent on one particular grain lying ahead of the crack tip. On the contrary, the crack tip traversed a large number of grains (~10) across the thickness of laminated polysilicon, which resulted in values for the effective K_{IC} that represented the average of the local K_{IC} of several grains through the specimen thickness. Due to the sampling of multiple grains at the crack front, the effective K_{IC} of laminated polysilicon was close to the average for Si (~0.9 MPa√m) and resulted in much tighter distribution of values.

Similar to MUMPs polysilicon [24], local heterogeneity in columnar polysilicon promoted crack arrest: for example, a specimen doped with 2% PSG, showed subcritical crack growth: the crack arrested at a GB after an initial advancement and then reinitiated at a higher load. Fig. 11(a) shows a pre-crack extending to the right hand side, and the fracture cross-section in Fig. 11(b). The AFM image in Fig. 11(d) shows the initial location of the crack tip. Upon an applied load of 5.15 mN, the pre-crack kinked through a grain at an angle with respect to the far field load and got arrested at the next grain. A drop in the load is noticed in the force vs. time plot in Fig. 11(c). In the initial crack advance, K_{IC} = 0.82 MPa√m, which lies at the lower bound of measured K_{IC} values. The crack resisted further loading up to 6.8 mN when the crack propagated catastrophically at K_{IC} = 1.1 MPa√m which is 25% higher than that for the first crack advance. This is generated by local variations in toughness due to the heterogeneous, anisotropic microstructure, as illustrated in the cohesive zone microstructural model by Foulk et. al [26]. It should be noted, that in addition to local variations in toughness, the arrested kinked crack in Fig. 11(b) required a larger far field force to reinitiate failure catastrophically due to local mode mixity which resulted in much higher apparent K_{IC}.

The K_{IC} of columnar polysilicon doped with 0.5% and 2% PSG content was 1.02±0.13 MPa√m and 1.05±0.14 MPa√m, respectively. These two doped columnar polysilicon K_{IC} values were 10% higher than the undoped toughness of 0.95±0.08 MPa√m. The standard deviation of measured values was also higher for doped polysilicon. During diffusion doping at high temperature (at 1050 °C), P atoms diffuse into the substitutional sites of a Si crystal [28], which can alter the cohesive law of Si thereby affecting the intrinsic critical stress intensity factor. The bond strength of P-Si (363.6 KJmol^{-1}) is 11% higher than that of Si-Si (326.86 KJmol^{-1}) and hence the energy release rate for polysilicon doped with P is higher than undoped Si [42]. On the other hand, the average K_{IC} for doped laminated polysilicon was close to the undoped material. Although the K_{IC} for doped laminated polysilicon was expected to increase due to higher bond strength of P-Si, the measured K_{IC} values were comparable to the undoped material. This may be attributed to higher GB content per unit volume in laminated polysilicon due to the smaller grain size that dilutes the concentration of P and as a result, the energy release rate of polysilicon is only moderately increased. Additionally, the crack front resided in combination of grains and GBs along the thickness of laminate polysilicon and hence an increase in the toughness of GBs did not have significant impact to the overall K_{IC}. The effective K_{IC} of doped columnar polysilicon was most frequently in the range of 1.1-1.2 MPa√m. These relatively high K_{IC} values compared to the undoped material were due to the combined effect of crack tip material anisotropy and doping. It is possible that the effect of doping on K_{IC} is overshadowed by its dependence on the location of crack tip which already varies in the broad range of 0.8-1.2 MPa√m. Thus, it can be concluded that the reduced tensile strength of doped columnar polysilicon is solely due to the larger defects forming as a result of heavy doping and not due to intrinsic effects, which, on the contrary, show that heavily doped columnar polysilicon is 10-20% tougher than the undoped material.

C. Fracture Mechanics Prediction of Mechanical Strength using Surface Flaw Data

In the absence of major volumetric flaws or notches in a brittle material, its strength in tension is limited by the surface roughness which acts as surface microcracks. With knowledge of K_{IC} and the spectrum of surface roughness of a brittle material, its fracture strength could be estimated using Linear Elastic Fracture Mechanics (LEFM). Using a finite element formulation, Raju and Newman [43] calculated the K_{IC} for various defect geometries in a finite body, such as an embedded elliptical crack, a semi-elliptical surface crack, Fig. 12(a,c), and a quarter elliptical edge crack, Fig. 12(b,d). From their results, analytical expressions were developed to compute K_{IC} for a finite body.

The K_I for the semi elliptical surface crack shown in Fig. 12(c) is given by

$$K_I = \sigma\sqrt{\pi\frac{a}{Q}}F_s\left(\frac{a}{t},\frac{a}{c},\frac{c}{b},\phi\right) \tag{8}$$

where σ is far field stress, Q is shape factor for an elliptical crack, and F_s is boundary correction factor for surface crack. The shape factor Q for an elliptical shaped flaw is approximated by:

$$Q = 1 + 1.464\left(\frac{a}{c}\right)^{1.65} \tag{9}$$

For $0 \le a/c \le 2$, $c/b < 0.5$ and $0 \le \phi \le \pi$, F_s is given by

$$F_s = \left[M_1 + M_2\left(\frac{a}{t}\right)^2 + M_3\left(\frac{a}{t}\right)^4\right] g f_\phi f_w \tag{10}$$

where M_i are curve fitting parameters, and g, f_w and f_ϕ are a curve fitting function, a finite width correction factor and an angular function, respectively, are given in [43]. Similarly, the K_I for a finite body with a quarter-elliptical edge crack, Fig. 12(b,d) is given by

$$K_I = \sigma\sqrt{\pi\frac{a}{Q}}F_c\left(\frac{a}{t},\frac{a}{c},\phi\right) \tag{11}$$

where Fc is the boundary correction factor for an edge crack. The shape factor for a quarter-elliptical shaped crack is same as that for a semi-elliptical crack in (10). The boundary correction factor Fc is given by

$$F_c = \left[M_1 + M_2\left(\frac{a}{t}\right)^2 + M_3\left(\frac{a}{t}\right)^4\right] g_1 g_2 f_\phi \tag{12}$$

For the following conditions: $0.2 \le a/c \le 2$, $a/t \le 1$, and $0 \le \square \le \pi/2$, the curve fitting parameter M_i, the curve fitting functions (g_1, g_2), and the angular function ($f_\square$) are given in [43].

The fracture strength of laminated and columnar polysilicon was estimated using (8) and (11), and AFM images that captured the flaw geometry. From 10 μm × 10 μm AFM topography images of laminated and columnar polysilicon, root mean square (RMS) surface roughness, average mean to valley, and mean to peak valley distances were measured and listed in Table 4. Even though the RMS surface roughness was uniform across all polysilicon films in the range of 8-10 nm, the average mean to valley and mean to peak valley distances were slightly larger in the case of undoped, 0.5% PSG doped columnar polysilicon and significantly larger in heavily doped columnar polysilicon. Similarly, the mean to valley and the maximum peak to valley roughness values for heavily doped columnar polysilicon were notably larger than that for the other materials, as shown in Fig. 13(a,b).

The AFM topography images shown in Fig. 14 revealed frequent minor grooves on the top surface of columnar polysilicon which were scarcely found on the laminated polysilicon. While the frequency of such surface defects present was not affected by dopant concentration in columnar and laminated polysilicon, heavy doping made the groves deeper in the case of columnar polysilicon alone. A 3-D image of such a surface defect in undoped laminated polysilicon and a cross-sectional height profile are shown in Fig. 15. This groove can be approximated as a semi-elliptical surface crack with a length ($2c$) of 1,200 nm and depth (a) of 25 nm. Surface defects with crack lengths more than 1,000 nm were uncommon in laminated polysilicon and, on average, they were ~500 nm long and 20-25 nm deep. However, the average length of such surface grooves in columnar polysilicon was 1,200 nm with an average depth of 30 nm for undoped and 40 nm for heavily doped material, as shown in Fig. 13(b).

The failure strength of laminated and columnar polysilicon was calculated by approximating the top surface grooves with semi-elliptical cracks and applying (8) for a semi-elliptical surface crack, with known K_{IC}. The K_{IC} for polysilicon varied in the range of 0.82-1.2 MPa$\sqrt{m}$. As a conservative estimate of mechanical strength using the analysis in (8)-(12), K_{IC} = 0.85 MPa$\sqrt{m}$ was used. This value is also the average K_{IC} between single crystal (100), (110), and (111) [19]. Comparisons between measurements and predictions for as-fabricated and ion milled specimens are provided in Table 5. The estimated strength of laminated polysilicon was 2.68 GPa which fell within the range of measured strength values (2-3 GPa). Since the size and presence of defects in a material are statistical in nature, a more accurate estimate for strength could be obtained by extensive imaging of defects. Similarly, the estimated strength of columnar polysilicon was 2.4 GPa and 2.1 GPa for undoped and doped polysilicon, which compared well with the strength of the corresponding films subjected to ion milling.

Fig. 8(a) and 9 pointed out that the largest crevices resided at the sidewalls of columnar polysilicon. Hence, in order to predict the fracture strength of polysilicon with critical sidewall defects, these flaws were approximated as quarter-elliptical edge cracks with lengths a and c, as shown in Fig. 12(b,d). The fracture strength is predicted using the K_{IC} relation for quarter-elliptical edge crack given in (11). SEM images were used to measure the approximate flaw geometry. From Fig. 8(a), the length c and depth a of the edge crack for heavily doped columnar polysilicon were 500 nm each. Similarly, for undoped columnar polysilicon, c and a were measured as 250 nm and 100 nm from Fig. 7(a,b). Since the sidewalls of laminated films were free of deep grooves, the strength was predicted by assuming the previously accounted surface crack as an edge crack, whose a and c are 25 nm and 500 nm. The strength of different polysilicon films was predicted in the presence of an edge crack and is compared in Table 6 with values measured from as-fabricated specimens. The strength predicted for laminated and columnar polysilicon films matched well with the measured values. This analysis again supports our previous discussion that the lower strength of columnar polysilicon was the result of deep sidewall grooves and crevices.

D. Strength of Columnar Polysilicon with Defect-free Sidewalls

The catastrophic flaws on the specimen edges of columnar polysilicon potentially could be eliminated with rapid etching after removal of the sacrificial oxide, or an extra step of oxidation of the specimen edge and subsequent etching of the oxide. In order to quantify the strength of columnar polysilicon in absence of sidewall defects, the sidewalls of the dog bone shaped specimens were trimmed and polished using a Focus Ion Beam (FIB). The specimen edges were milled using 7 nA probe current to obtain smooth sidewalls, as shown in Fig. 16(a,b). Subsequently, the sacrificial oxide layer was etched in 49% HF to obtain freestanding specimens for mechanical testing. A comparison between the as-deposited and processed sidewalls can be obtained by referring to Fig. 9 and 16(b). The fracture strength of columnar and laminated polysilicon with smooth sidewalls is compared with as-deposited polysilicon and as a function of doping in Fig. 17. The average strength of columnar polysilicon with smooth sidewalls was in the range of 1.9-2.3 GPa, i.e. 70-100% higher than as-fabricated columnar polysilicon. However, the average strength of laminated polysilicon with smooth sidewalls was measured as 2.2 GPa which is 10-15% lower than its as-deposited sidewall specimens. This indicates that the strength measured for polysilicon with FIBed-sidewalls is limited by defects introduced during ion milling process at the fillet locations. Therefore, columnar polysilicon films with defect-free sidewalls could withstand stresses beyond 2.2 GPa. It is also inferred from this experiment, that the strength of columnar polysilicon with smooth sidewalls could be very similar to that of laminated polysilicon.

Finally, the characteristic strengths of laminated and columnar polysilicon measured in this work and [33] are compared in Fig. 18 with that of the corresponding polysilicon layers fabricated using Sandia's standard SUMMiT V^{TM} [8] process. As shown, the characteristic strength of the Poly1 layer could be enhanced by 40-150% by controlling the microstructure of polysilicon as described in this paper. As a result, if Poly1 was fabricated as a laminated structure, it could have a characteristic strength as high as that of the Poly4 layer which has been reported to be the strongest of all

polysilicon layers of the SUMMiT V^{TM} process due to its reduced surface roughness.

V. Conclusion

The effects of microstructure and doping on the tensile strength of polysilicon were investigated using columnar and laminated polysilicon films subjected to different doping conditions. Heavy doping lowered the strength of columnar polysilicon by more than 20%, but had minimal effect on the strength of laminated polysilicon. The reduction in strength of columnar polysilicon was due to large sidewall defects that formed during annealing and P diffusion, and acted as stress concentrations. While these defects were more pronounced in the polysilicon doped with 2% PSG, they were not found in 0.5% PSG doped films, which provides a critical concentration for P beyond which the defect formation is accelerated. The presence of P doping actually had a beneficial effect on the "intrinsic" toughness of polysilicon: The average effective K_{IC} of columnar polysilicon subjected to heavy P doping was the highest among all films, and 10% higher than the undoped columnar material. Due to material anisotropy at the crack tip, the K_{IC} varied by as much as 25% from sample to sample for each type of columnar polysilicon, due to sampling of different grain configurations. On the contrary, the effective K_{IC} of laminated polysilicon varied in a narrow range, due to the averaging effect of the different grain orientation in each layer at the crack front. The calculated Weibull parameters could accurately predict the characteristic strength of 180 times smaller polysilicon specimens with the same grain size and doping, and *vice versa*, assuming that all critical flaws lie in the specimen sidewalls. Notably, the strength of columnar polysilicon with defect-free sidewalls increased by 70-100%, after eliminating the sidewall flaws by ion milling.

Acknowledgment

The authors thank M.J. Shaw at Sandia National Labs for coordinating the fabrication of these custom polysilicon materials. Additionally, we thank the staff at Material Research Laboratory, University of Illinois at Urbana Champaign for their extended help during the usage of SEM, AFM and FIB. BLB was supported by the Department of Energy, Office of Basic Energy Sciences. Sandia National Laboratories is a multi-program laboratory managed and operated by Sandia Corporation, a wholly owned subsidiary of Lockheed Martin Corporation, for the U.S. Department of Energy's National Nuclear Security Administration under contract DE-AC04-94AL85000.

References

[1] http://mems.sandia.gov/gallery/images.html

[2] A. McCarty, I. Chasiotis, "Description of brittle failure of non-uniform MEMS geometries", *Thin Solid Films*, vol. 515, pp. 3267-3276, 2007

[3] I. Chasiotis, W.G. Knauss, "The mechanical strength of polysilicon films: Part 2. Size effects associated with elliptical and circular perforation", *J. Mechanics and Phys. Solids*, vol. 51, no. 8, pp. 1551-15, 2003

[4] D.C. Miller, B.L. Boyce, P.G. Kotula, C.R. Stoldt, "Connections between morphological and mechanical evolution during galvanic corrosion of micromachined polycrystalline and monocrystalline silicon", *J. Appl. Phys.*, vol. 103, 123518, 2008.

[5] T. Alan, M.A. Hines, A.T. Zehnder, "Effect of surface morphology on the fracture strength of silicon nanobeams", *Appl. Phys. Lett.*, vol. 89, no. 9, Art. no. 091901, 2006

[6] W. Sharpe Jr., K. Jackson, J. Hemker, Z. Xie, "Effect of specimen size on young's modulus and fracture strength of polysilicon", *J. Microelectromech. Syst.,* vol. 10, no. 3, pp. 317-326, 2001

[7] J. Koskinen, J. Steinwall, R. Soave, H. Johnson, "Microtensile testing of free-standing polysilicon fibers of various grain sizes", *J. Micromech. Microeng.*, vol. 3, no. 1, pp. 13-17, 1993

[8] B.L. Boyce, J.M. Grazier, T.E. Buchheit and M.J. Shaw, "Strength distributions in polycrystalline silicon MEMS", *J. Microelectromech. Syst.*, vol. 16, no. 2, pp. 179-190, 2007

[9] S.S. Hazra, M.S. Baker, J.L. Beuth, M.P. De Boer, "Demonstration of an in situ on-chip tensile tester", *J. Micromech. Microeng.*, vol. 19, no. 8, art. no. 082001, 2009

[10] E.D. Reedy Jr., B.L. Boyce, J.W. Foulk III, R.V. Field Jr.,M.P. de Boer, and S.S. Hazra, "Predicting fracture in micrometer-scale polycrystalline silicon MEMS structures", *J. Microelectromech. Syst.*, vol. 20, no. 4, pp.922-932, 2011

[11] W. Sharpe Jr, K. Jackson, K. Hemker, and Z. Xi, " Effect of specimen size on Young's modulus and fracture strength of polysilicon", *J. Microelectromech. Syst*., vol. 10, pp. 317-326, 2001

[12] I. Chasiotis, "Mechanics of thin films and microdevices", IEEE Trans. Device Mater. Rel., vol. 4, no. 2, pp. 176-188, 2004

[13] I. Chasiotis, W.G. Knauss, "The mechanical strength of polysilicon films: Part 1. The influence of fabrication governed surface conditions", *J. Mechanics and Phys. Solids*, vol. 51, pp. 1533-1550, 2003

[14] H. Kahn, C. Deeb, I. Chasiotis, and A.H. Heuer, "Anodic oxidation during MEMS processing of silicon and polysilicon: native oxides can be thicker than you think", *J. Microelectromech. Syst*., vol 14, no. 5, pp. 914-923, 2005

[15] R. Ballarini, H. Kahn, N. Tayebi, and A.H. Heuer, "Effects of microstructure on the strength and fracture toughness of polysilicon: A wafer level testing approach," *ASTM special tech. pub.*, vol. 1413, pp. 37-51, 2001

[16] T. Tsuchiya, J. Sakata and Y. Taga, "Tensile strength and fracture toughness of surface micromachined polycrystalline silicon thin films prepared under various conditions" *MRS Symp. Proc.*, vol. 505 , pp. 285-290, 1997

[17] T. Kammins, "Structure", in *Polycrystalline silicon for integrated circuits and displays*, 2nd ed., Kluwer Acadamic Publishers, pp. 103-114

[18] F. Ebrahimi, and L. Kalwani, "Fracture anisotropy in silicon single crystal", *Mater. Sci. Eng. A*, vol. 268, no. 1-2, pp. 116-126, 1999

[19] C.P. Chen, and M.H. Leipold, "Fracture toughness of silicon", *Amer. Cer. Soc. Bulletin*, vol. 59, pp. 519, 1980

[20] Y. Tsai and J. Mecholsky, "Fractal fracture of single crystal silicon", *J. Mater. Resources*, vol. 6, pp. 1248–1263, 1991

[21] A.M. Fitzgerald, R.H. Dauskardt and T.W. Kenny, "Fracture toughness and crack growth phenomena of plasma-etched single crystal silicon", *Sens. and Actuat. A*, 83, pp. 194–199, 2000

[22] H. Kahn, N. Tayebi, R. Ballarini, R.L. Mullen, and A.H. Heuer, "Fracture toughness of polysilicon MEMS devices", *Sens. Actuat. A: Phys.*, vol. 82, no. 1-3, pp. 274-280, 2000

[23] J. Bagdahn, J. Schischka, M. Petzold, and W.N. Sharpe Jr., "Fracture toughness and fatigue investigations of polycrystalline silicon", *Proc. of SPIE - The Inter. Soc. Opt. Eng.,* vol. 4558, pp. 159-168, 2001

[24] I. Chasiotis, S.W. Cho, and K. Jonnalagadda, "Fracture toughness and subcritical crack growth in polycrystalline silicon", *J. Appl. Mech.*, vol. 73, no. 5, pp. 714-722, 2006

[25] S.W. Cho, K. Jonnalagadda, and I. Chasiotis, "Mode I and mixed mode fracture of polysilicon for MEMS", *Fatigue and Fracture of Eng. Mater. Struct.*, vol. 30, no. 1, pp. 21-31, 2007

[26] J.W. Foulk, III, G.C. Johnson, P.A. Klein, and R.O. Ritchie, "A micromechanical basis for partitioning the evolution of grain bridging in brittle materials", *J. Mech. Phys. Solids*, vol. 55, no. 4, pp. 719-743, 2007

[27] J.W. Foulk, III, G.C. Johnson, P.A. Klein, and R.O. Ritchie, "On the toughening of brittle materials by grain bridging: Promoting intergranular fracture through grain angle, strength, and toughness", *J. Mech. Phys. Solids*, vol. 56, no. 6, pp. 2381-2400, 2008

[28] Z. Zeng, X. Ma, J. Chen, Y. Zeng, D. Yang, and Y. Liu, "Effects of heavy phosphorus-doping on mechanical properties of Czochralski silicon", *J. Appl. Phys.*, vol. 107, no. 12, pp. 123503-1-5, 2010

[29] J. G. Swadener and M. Nastasi, "Effect of dopants on the fracture toughness of silicon", *J. Mater. Sci. Lett.*, vol. 21, no. 17, pp. 1363-1365, 2002

[30] K. Park, S. Batra and S. Banerjee, "Role of negatively charged vacancies in secondary grain growth in polycrystalline silicon during rapid thermal annealing", *Appl. Phys. Lett.*, vol. 58, pp. 2414-2416, 1991

[31] V.P. Lesnikova, A.S. Turtsevich, V.Y. Krasnitsky, V.A. Emelyanov, O.Y. Nalivaiko, S.V. Kravtsov and T.V. Makarevich, "The structure, morphology and resistivity of in situ phosphorus doped polysilicon films", *Thin Solid Films*, vol. 247, pp. 156-161, 1994

[32] R. Plugaru, E. Vasile, C. Cobianu and D. Dascalu, "Investigation of the surface of P-implated LPCVD silicon films", Mater. Sci. Eng. B, vol. 42, pp. 240-242, 1996

[33] B.L. Boyce, M.J. Shaw, P. Lu, and M.T. Dugger, "Stronger silicon for microsystems", *Acta Materialia*, vol. 58, pp. 439–448, 2010

[34] J. J. Sniegowski and M. P. de Boer, "IC-compatible polysilicon surface micromachining", *Annual Rev. Mater. Sci.*, vol. 30, pp. 299-333, 2000

[35] S.W. Cho and I. Chasiotis, "Elastic Properties and Representative Volume Element of Polycrystalline Silicon for MEMS", *Exper. Mech.*, vol. 47, no. 1, pp. 37-49, 2007

[36] K. Jonnalagadda, I. Chasiotis, S. Yagnamurthy, J. Lambros, J. Pulskamp, R. Polcawich, and M. Dubey, "Experimental investigation of strain rate dependence of nanocrystalline Pt films", *Exper. Mech.*, vol. 50, pp. 25-35, 2010

[37] H. Tada, P. C. Paris, and G. R. Irwin, "The stress analysis of cracks handbook", 3rd ed., ASME Press, New York, pp. 52–53, 2000

[38] A. Hallinan Jr., "A review of the Weibull distribution", *J. Quality Tech.*, vol. 25., no. 2, pp. 85-93, 1993

[39] W.M. Robertson, "Thermal etching and grain-boundary grooving of silicon ceramics", *J. Amer. Cer. Soc.*, vol. 64, no. 1, pp. 9-13, 1981

[40] Y. Wada and S. Nishimatsu, "Grain growth mechanism of heavily phosphorus implanted polycrystalline silicon", *J. Electrochem. Soc.*, vol. 125, no. 9, pp. 1499-1504, 1978

[41] M. Steyer, A. Dastgheib-Shirazi, H. Wagner, G. Micard, P.P. Altermatt, and G. Hahn, "A study of various methods for the analysis of the phosphosilicate glass layer", *27th European Photovoltaic Solar Energy Conf. Exhib. in Frankfurt, Germany*, pp. 1325-1328, 2012

[42] D.R. Lide, "Handbook of chemistry and physics", 85th Ed, CRC Press LLC

[43] J.C. Newman and I.S Raju, "Stress intensity factor equations for cracks in three-dimensional finite bodies", ASTM STP791-EB / STP37074S, 1983

FIGURES

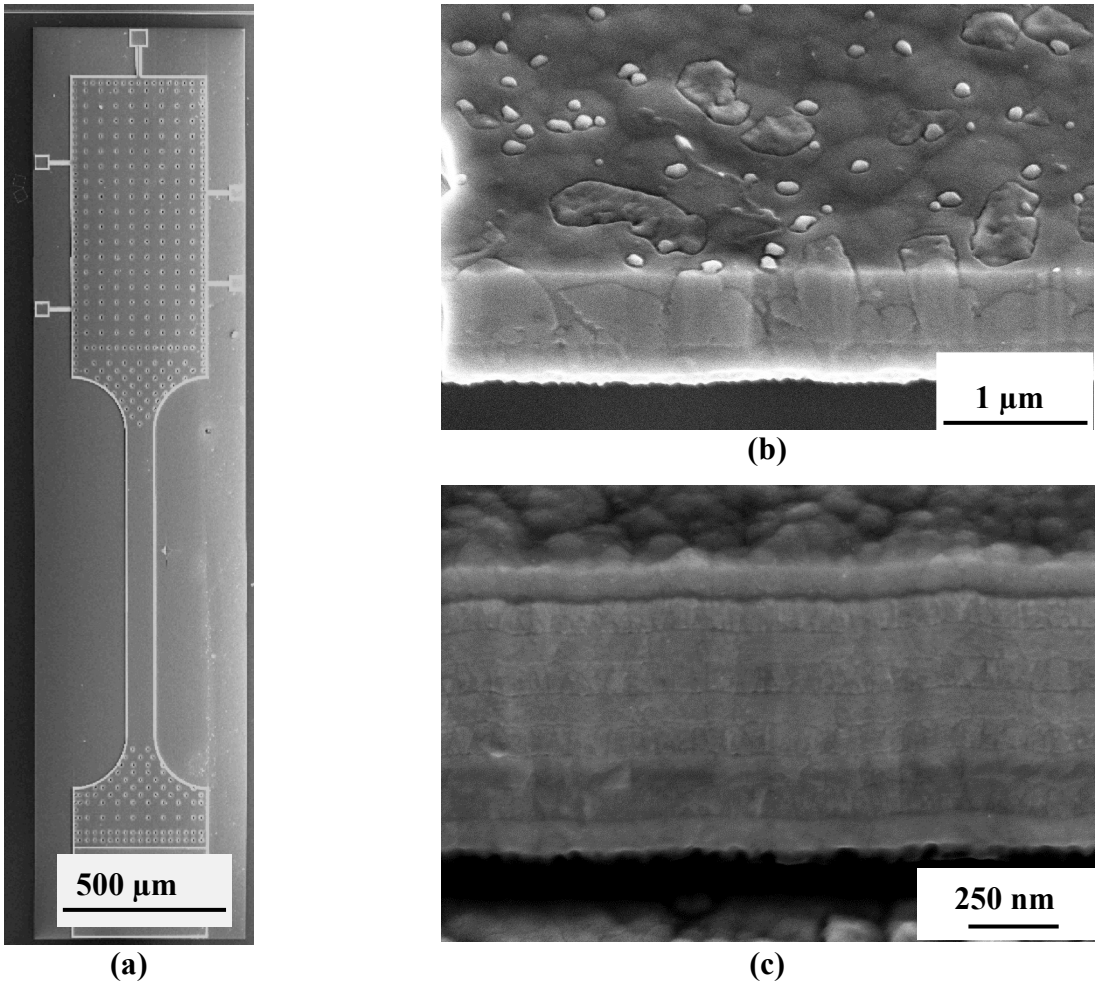

Fig. 1. (a) Uniaxial tension specimen, and cross section of undoped **(b)** columnar, and **(c)** laminated polysilicon.

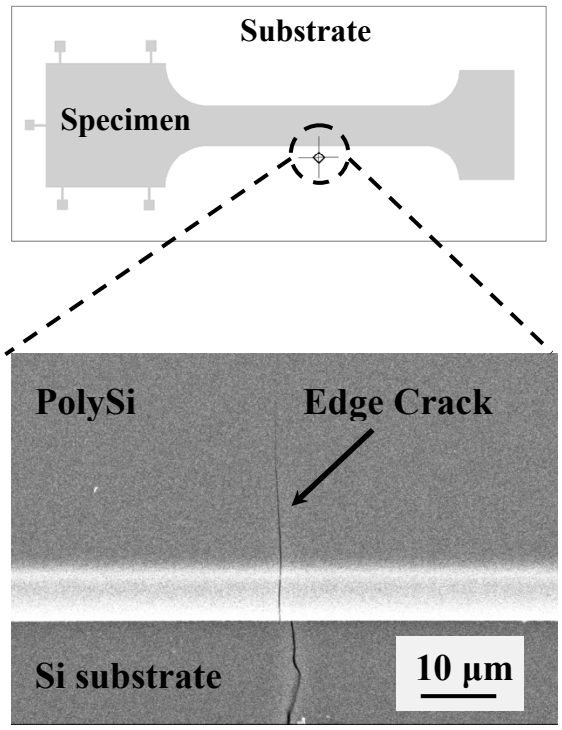

(a)

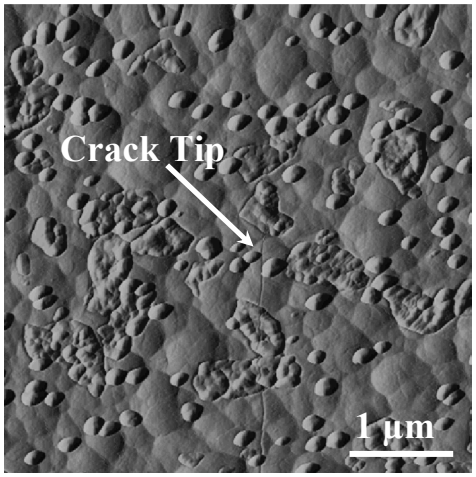

(b)

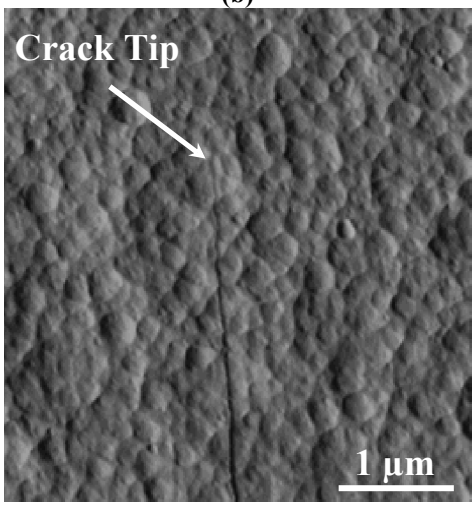

(c)

Fig. 2. (a) Prefabricated edge crack, AFM image of crack tip in: **(b)** columnar grain polysilicon, and **(c)** laminated polysilicon.

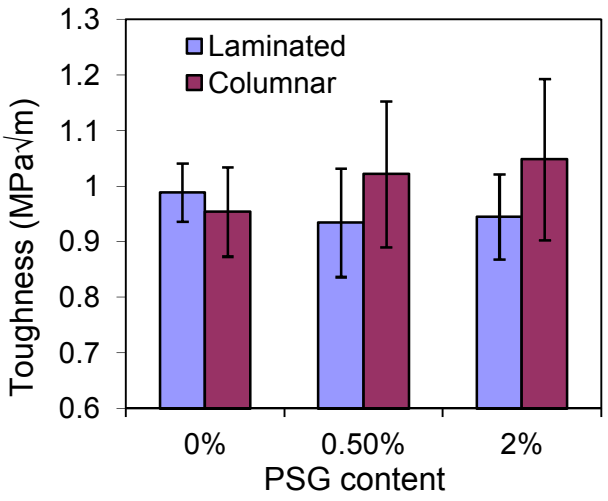

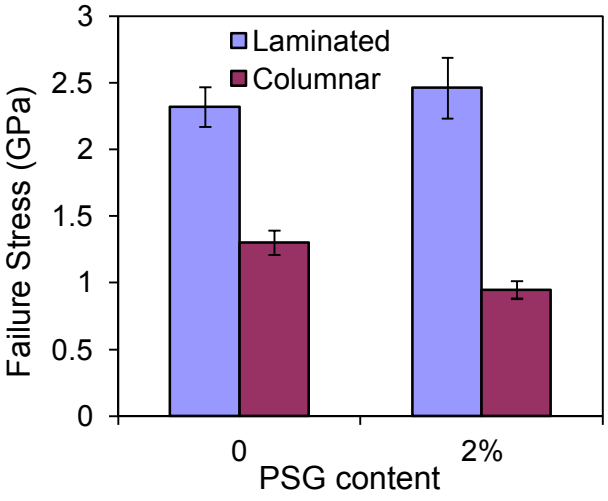

Fig. 3. K_{IC} for laminated and columnar grain polysilicon vs. P doping. The error bars represent one standard deviation.

Fig. 4. Tensile strength of columnar and laminated polysilicon doped with 0% and 2% PSG. The error bars represent one standard deviation.

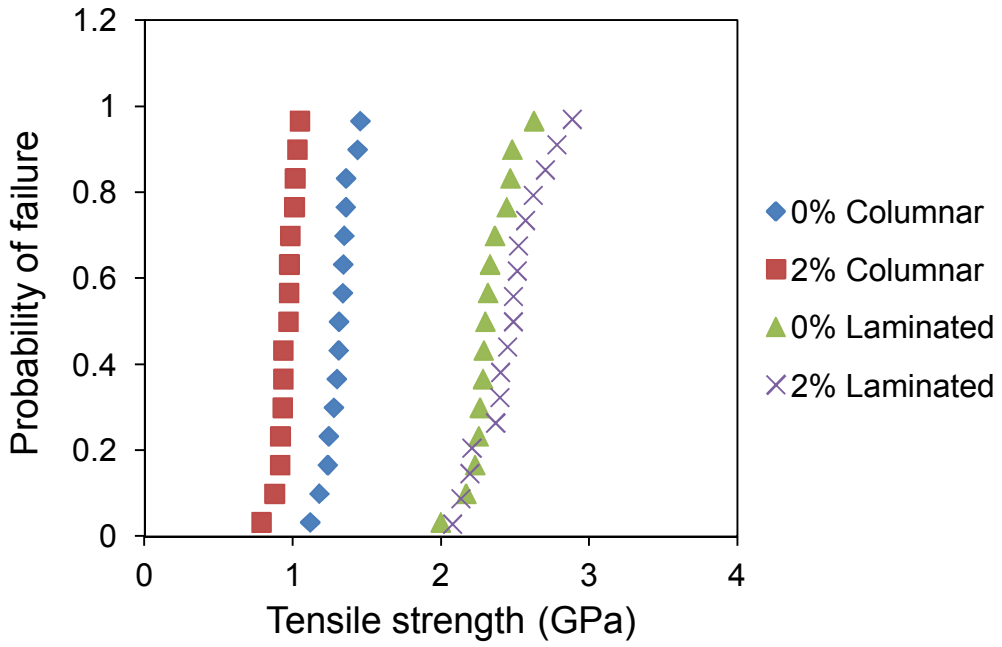

Fig. 5. Probability of failure vs. tensile strength for columnar and laminated polysilicon films.

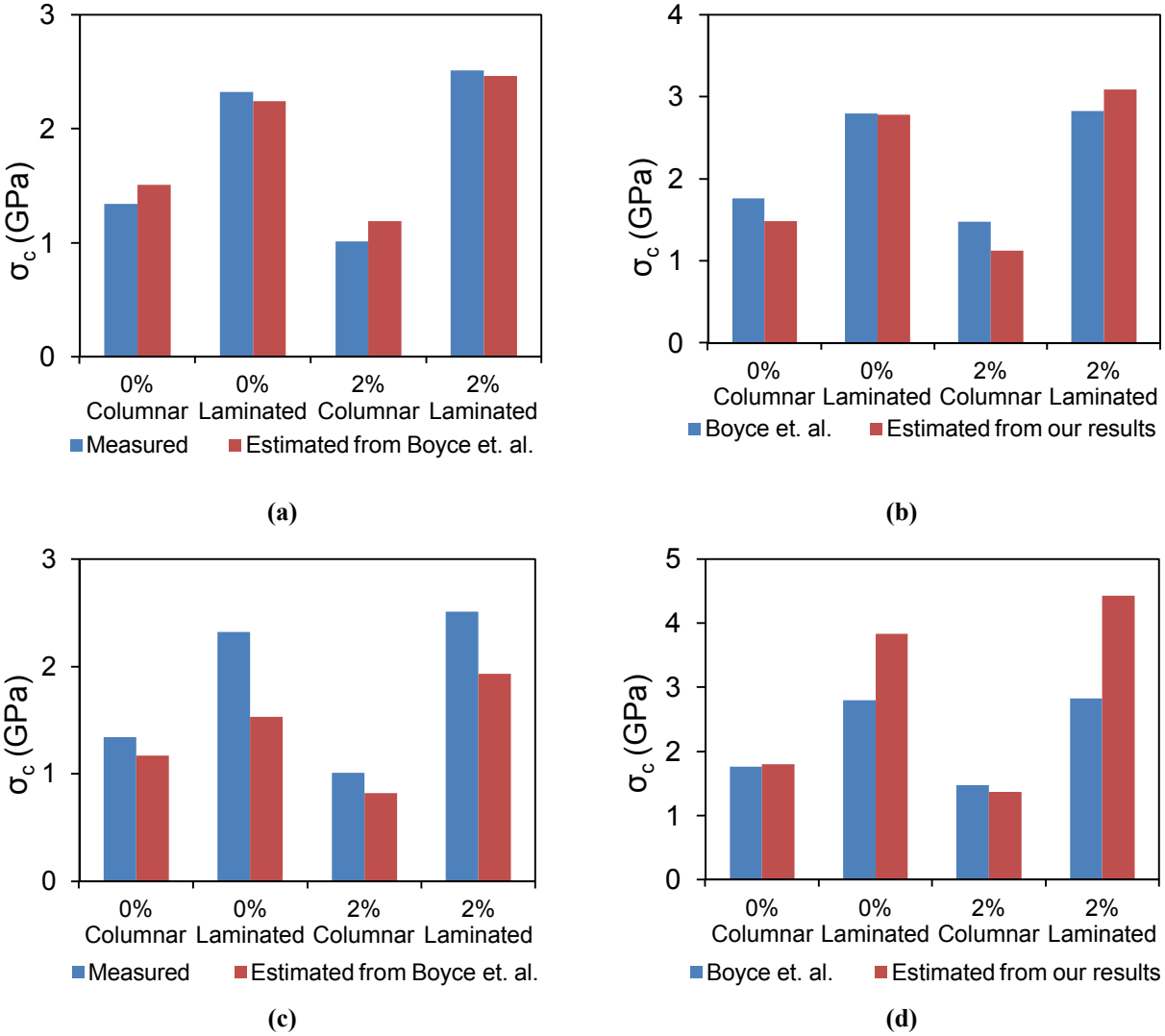

Fig. 6. Estimation of characteristic strength of large and small specimens using data from small and large specimens, respectively, assuming that all critical flaws lie in the **(a-b)** sidewall area, and **(c-d)** top surface area.

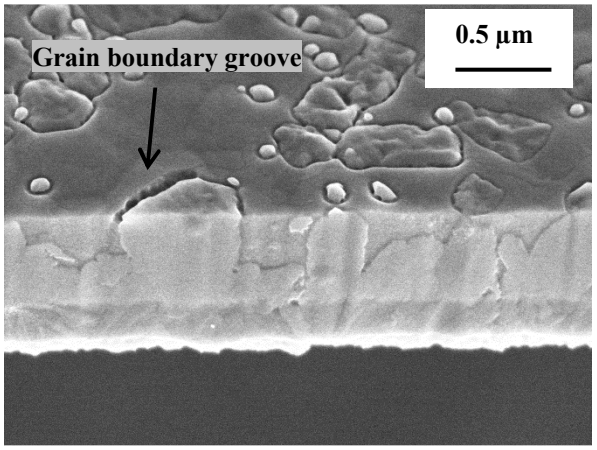

(a)

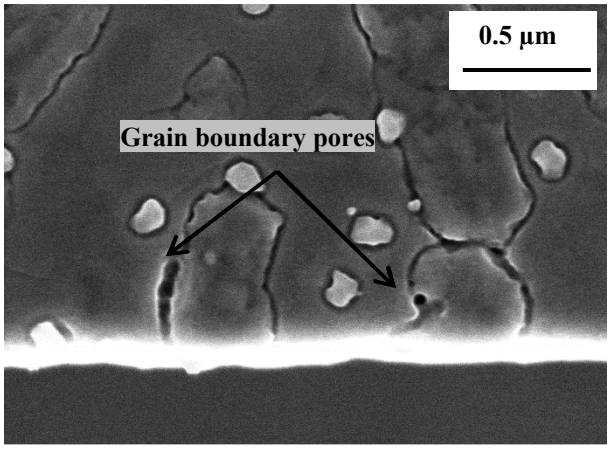

(b)

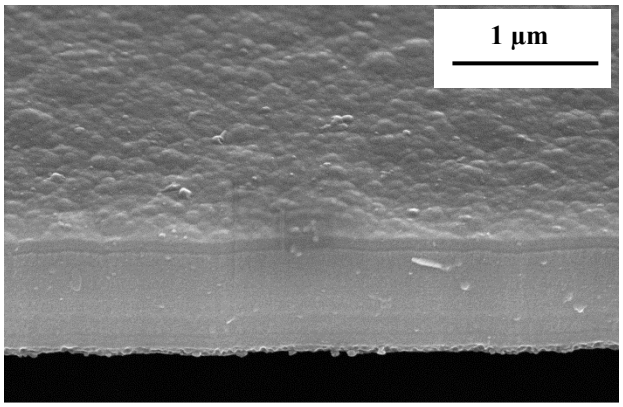

(c)

Fig. 7. SEM images of the sidewall and top specimen surface of **(a,b)** undoped columnar, and **(c)** undoped laminated polysilicon, respectively.

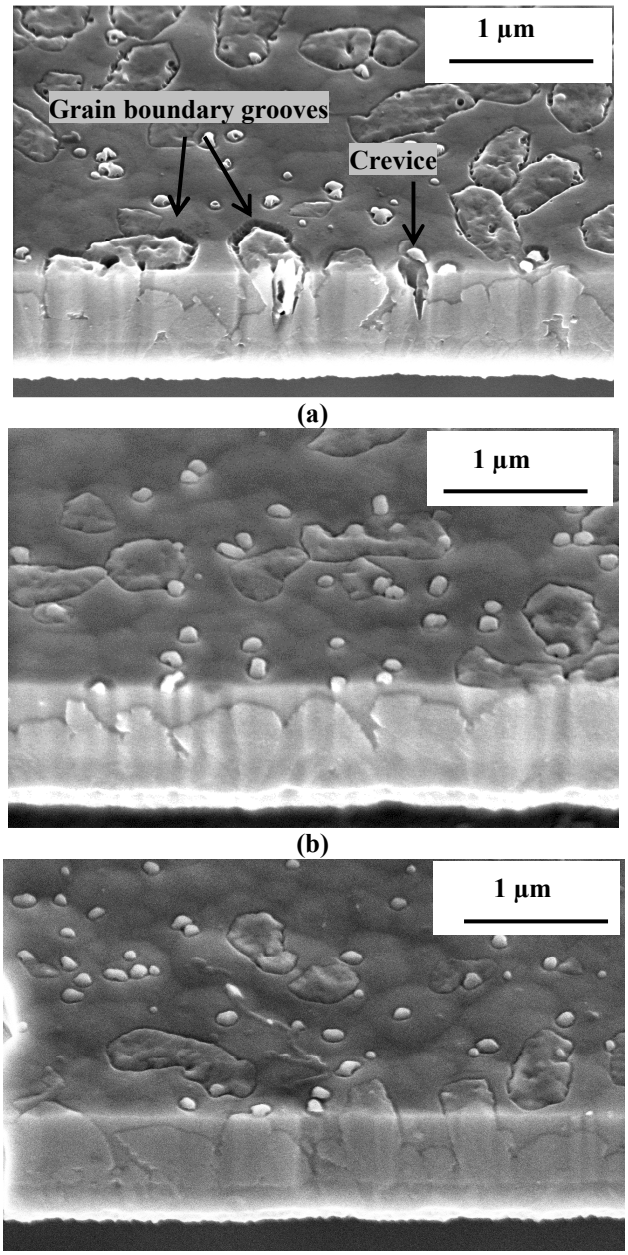

Fig. 8. Top surface and sidewall of **(a)** 2% PSG doped, **(b)** 0.5% PSG doped, and **(c)** undoped columnar polysilicon, after etching in 49% HF.

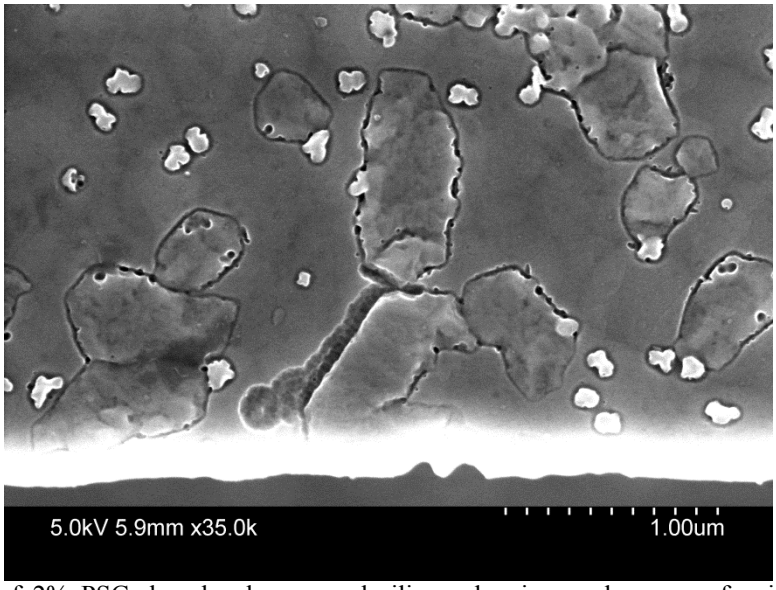

Fig. 9. Top surface of 2% PSG doped columnar polysilicon showing coalescence of voids at a GB near the sidewalls.

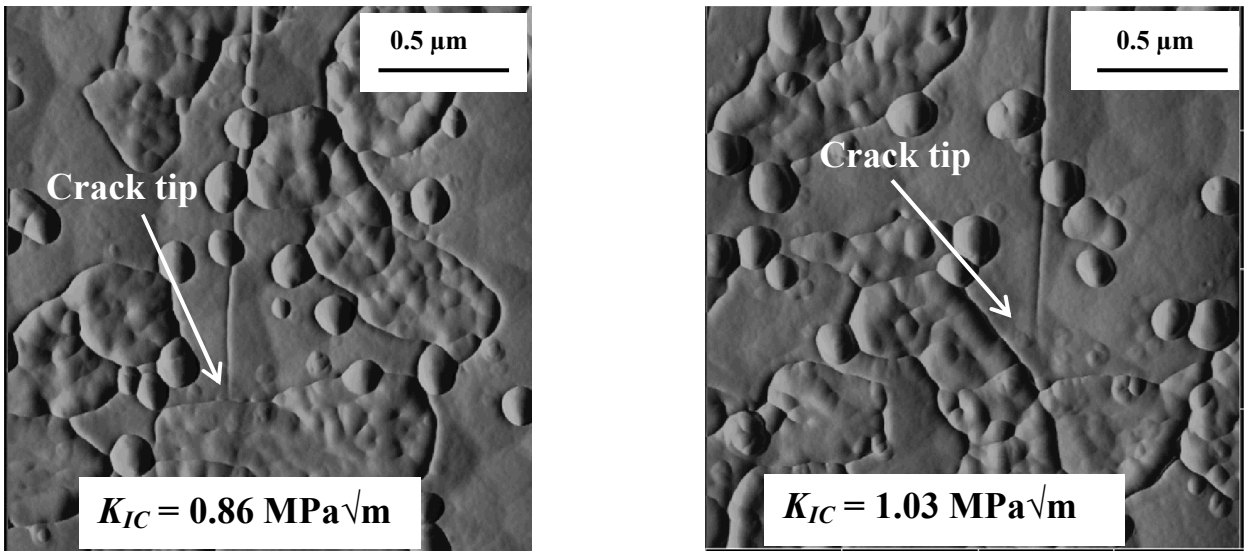

(a) **(b)**

Fig. 10. AFM images of columnar polysilicon with crack tip located **(a)** at a GB, and **(b)** within a grain and in front of a triple junction.

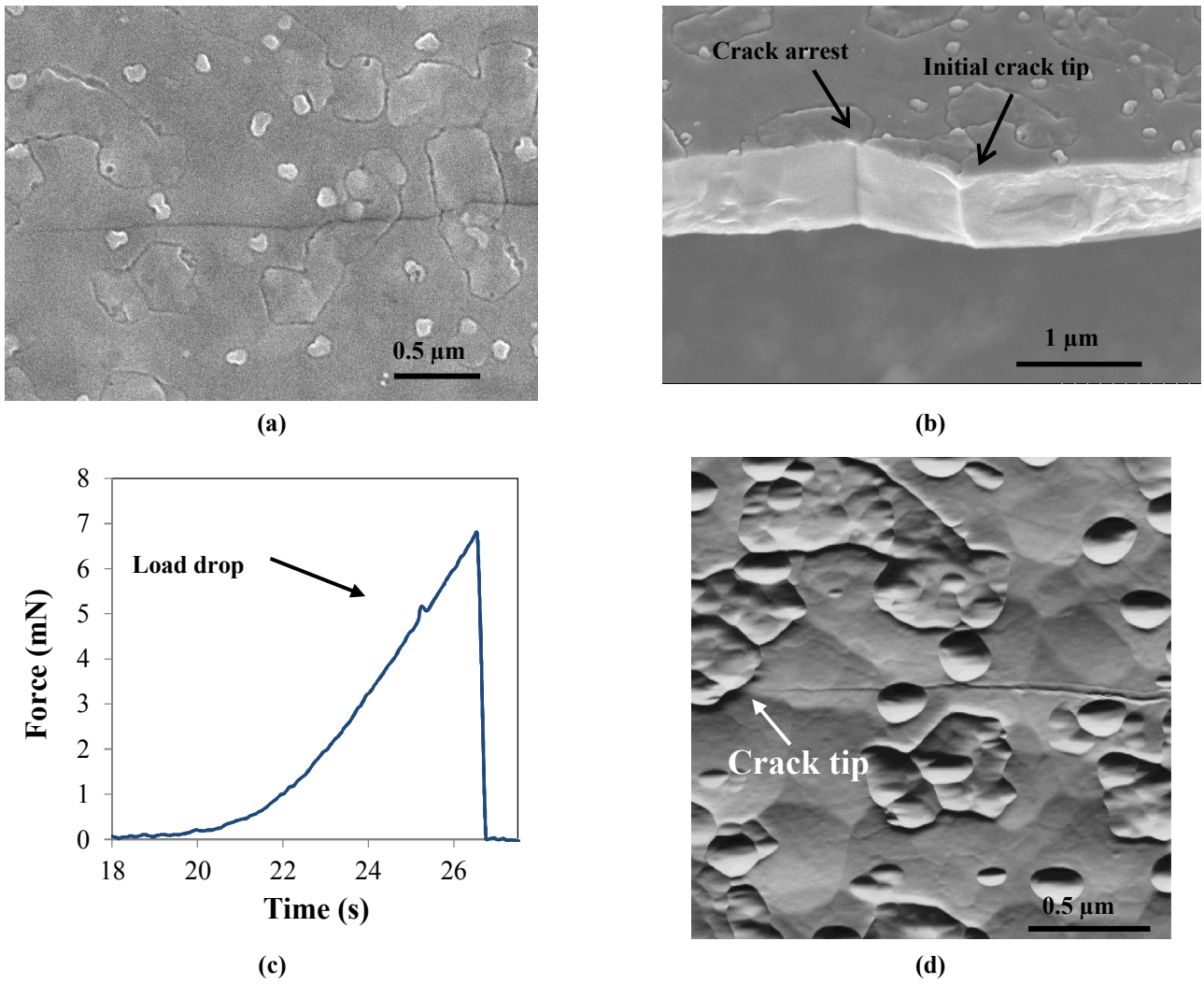

Fig. 11. **(a,b)** SEM image of fracture cross sections and top view of the crack in heavily doped columnar polysilicon, **(c)** far-field force vs. time during loading, and **(d)** pre-crack tip.

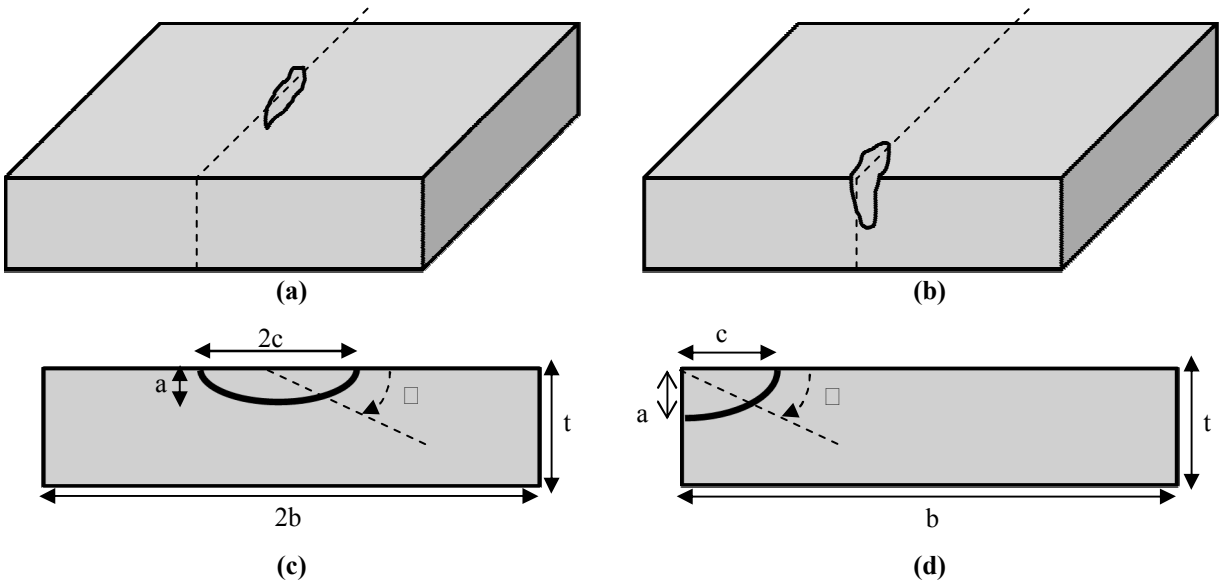

Fig. 12. Schematic of **(a)** semi elliptical surface crack, **(b)** quarter elliptical edge crack, and **(c-d)** the corresponding

cross sectional views.

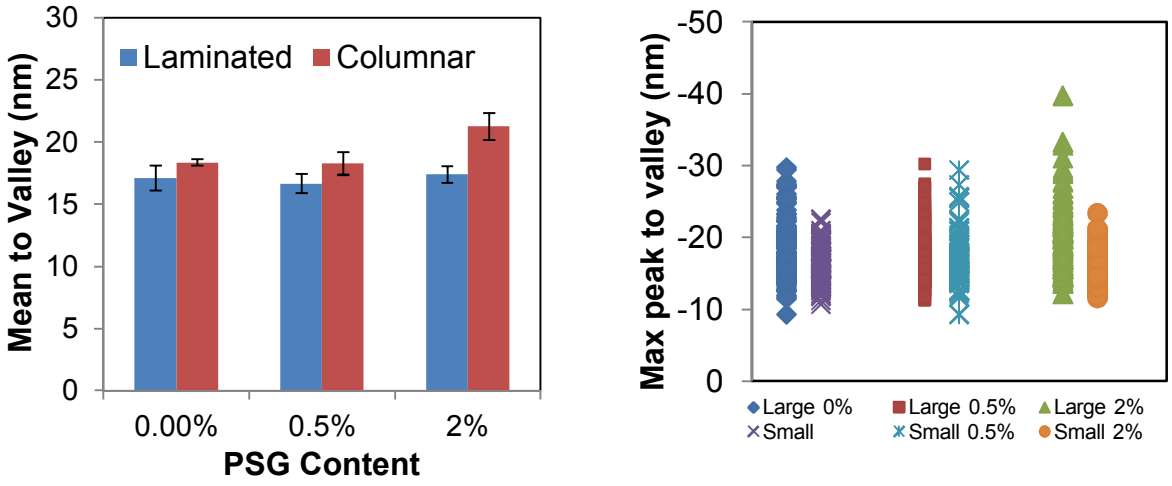

(a) **(b)**

Fig. 13. (a) Mean to valley roughness that is maximum for heavily doped polysilicon, and (b) maximum peak to valley roughness measured from 3 different 10 μm × 10 μm areas by AFM.

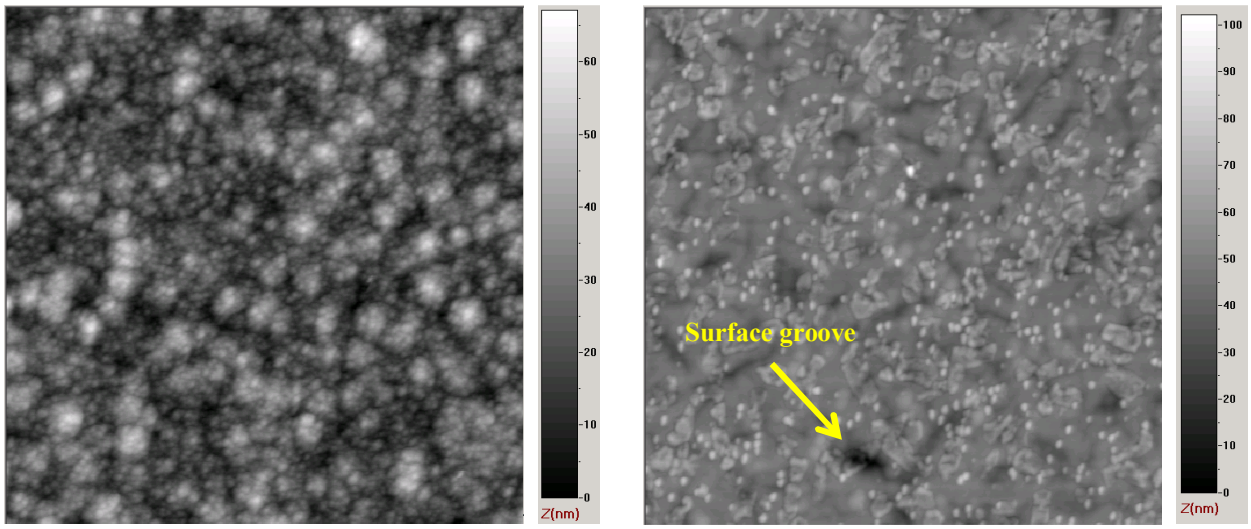

(a) **(b)**

Fig. 14. AFM topography images of **(a)** undoped laminated, and **(b)** undoped columnar polysilicon.

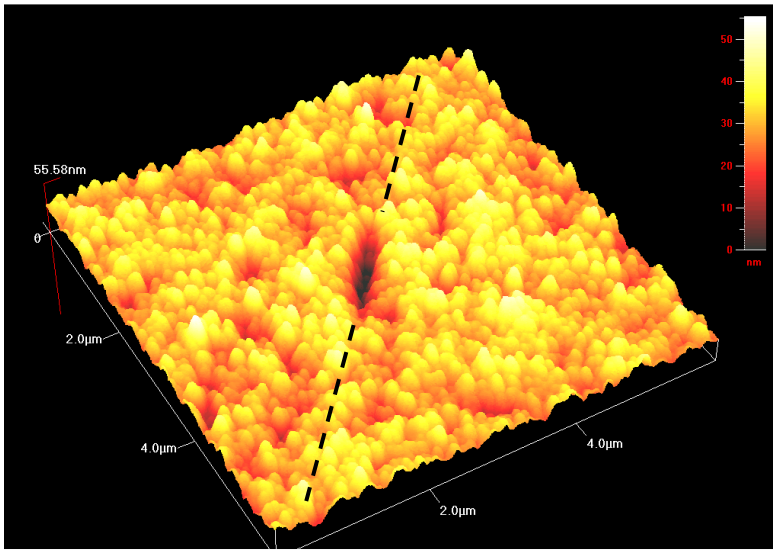

(a)

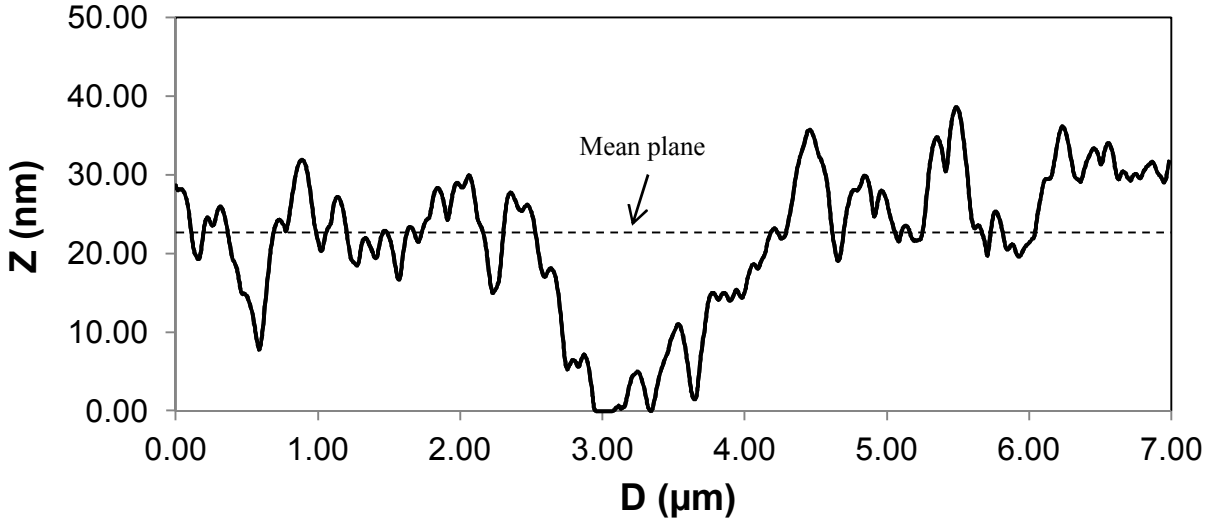

(b)

Fig. 15. (a) 3-D topography of undoped laminated polysilicon obtained by AFM, and **(b)** height profile at the cross-section indicated in (a).

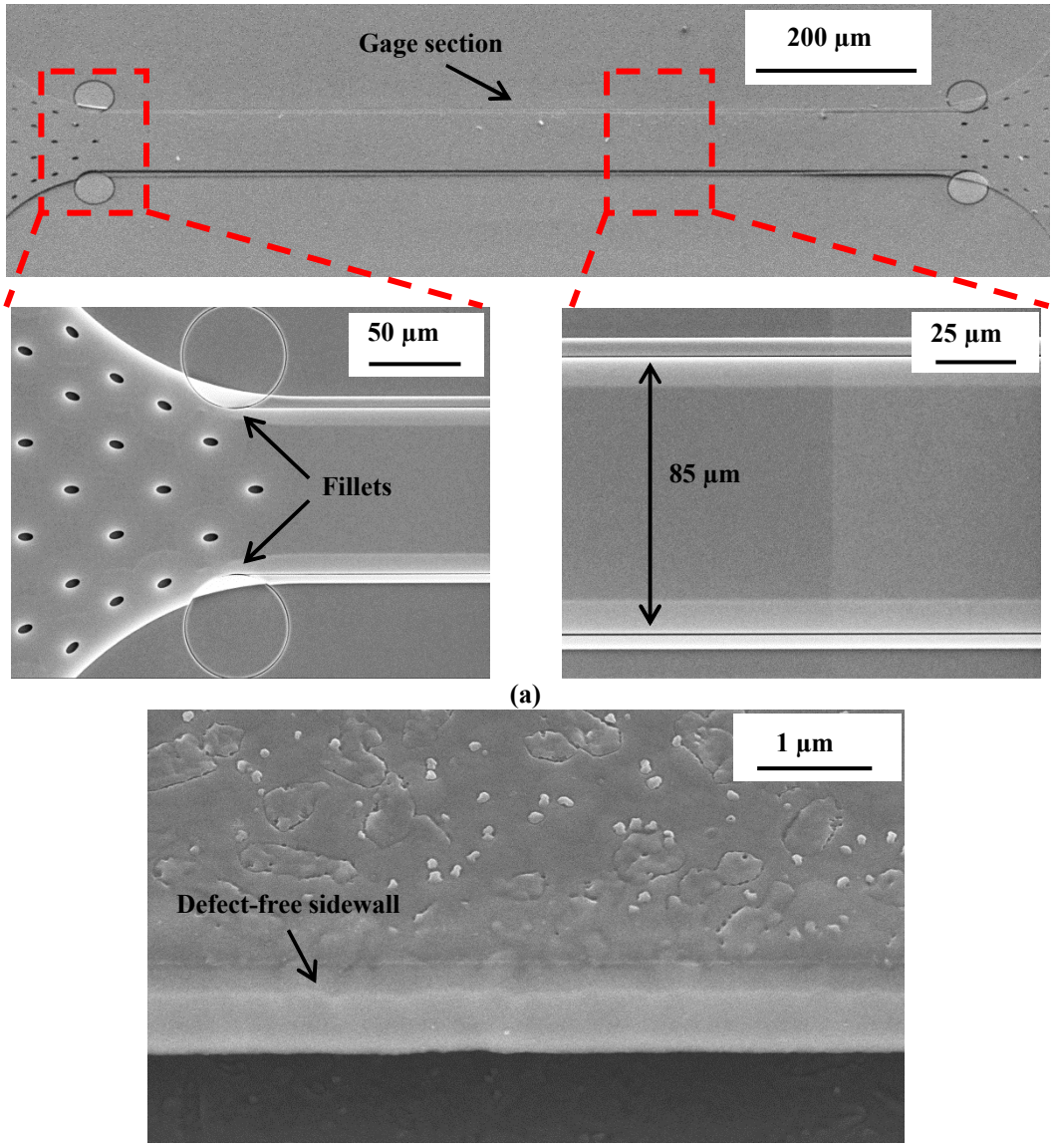

Fig. 16. (a) SEM images of FIB-machined specimen showing the gage section, the round fillets at the gage end, and the trimmed specimen edges. **(b)** Cross-sectional image of the defect-free sidewall after ion beam milling.

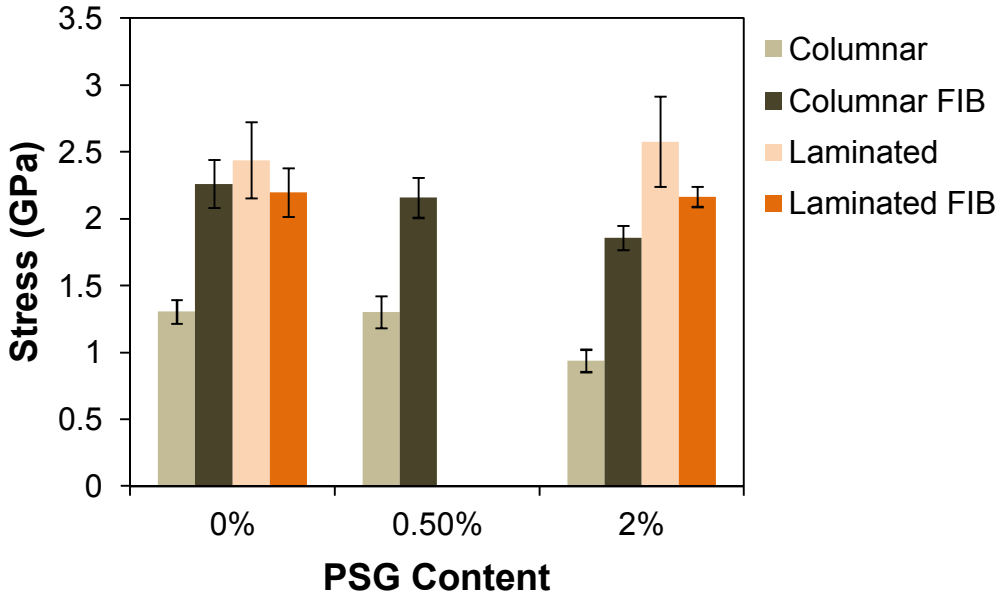

Fig. 17. Comparison of average fracture strength of as-deposited polysilicon and polysilicon with smoothed sidewalls using FIB. The error bars represent ±1 standard deviation.

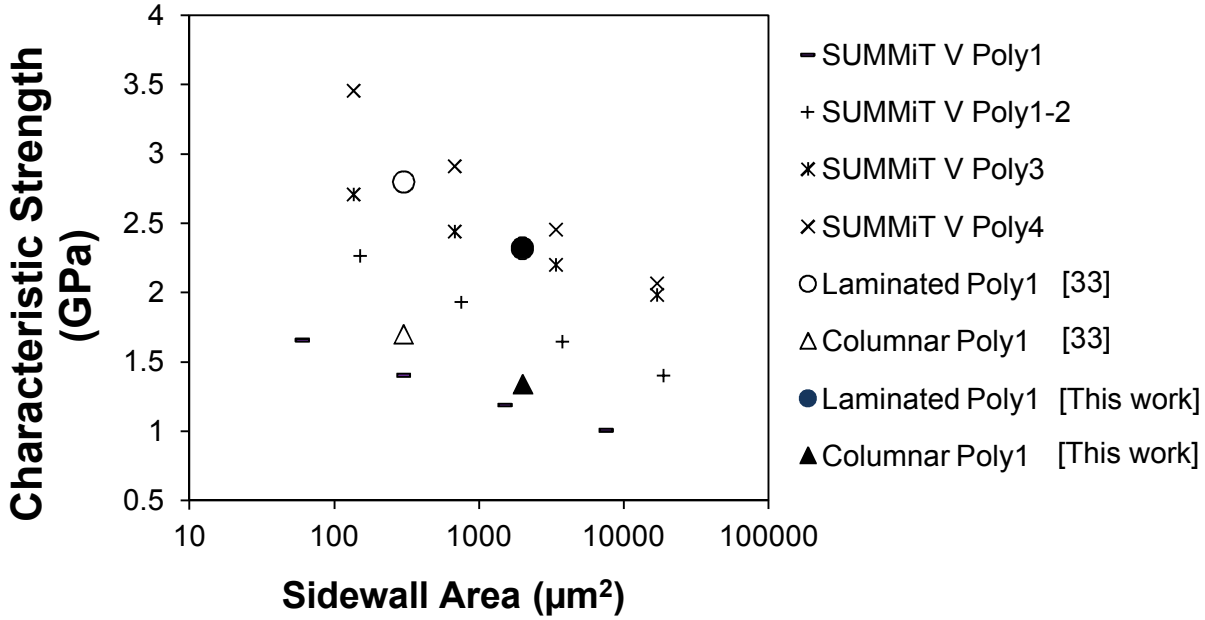

Fig. 18. Comparison of characteristic strength of polysilicon measured in this work, with various Poly layers fabricated by the standard SUMMiT V™ process. The sidewall area of the specimens tested in this work was 2,000 μm^2. The characteristic strengths of Poly1, Poly1-2, Poly3, Poly4 were calculated using (7), and the Weibull modulus and characteristic strength reported in [8] for specimens with gage surface area of 1,000 μm^2.

TABLES

Table 1. K_{IC}, strength and Young's modulus for columnar grained and laminated polysilicon doped with different concentrations of P. The average value ±1 standard deviation is presented.

Specimen type	K_{IC} (MPa√m)	Failure strength (GPa)	Young's modulus (GPa)
Undoped, Laminated	0.99±0.05	2.32±0.15	154.8±3.6
0.5% PSG, Laminated	0.94±0.10	-	-
2% PSG, Laminated	0.95±0.08	2.46±0.22	153.4±11.3
Undoped, Columnar	0.95±0.08	1.30±0.09	155.2±2
0.5% PSG, Columnar	1.02±0.13	1.30±0.12	157.0±1.2
2% PSG, Columnar	1.05±0.14	0.95±0.07	157.2±1.8

Table 2. Weibull strength and modulus of polysilicon calculated using two and three parameters.

Specimen	2 parameter Weibull		3 parameter Weibull		
	σ_c (GPa)	m	σ_c (GPa)	m	σ_u (GPa)
Undoped, Laminated	2.32	10.31	2.38	6.76	1.45
2% PSG, Laminated	2.51	9.09	2.55	8.36	0.9
Undoped, Columnar	1.34	17.63	1.34	9.31	0.6
2% PSG, Columnar	1.01	16.89	0.98	13.15	0.2

Table 3. Weibull parameters of the polysilicon measured here and by Boyce *et al*. [33].

Specimen	This work Dimensions – 1000×100×1 μm^3		Boyce *et al* [33] Dimensions ~ 150×3.75×1 μm^3	
	σ_c (GPa)	m	σ_c (GPa)	m
Undoped, Laminated	2.32	10.31	2.80	8.6
2% PSG, Laminated	2.51	9.09	2.83	13.5
Undoped, Columnar	1.34	17.63	1.76	12.9
2% PSG, Columnar	1.01	16.89	1.48	8.7

Table 4. Surface roughness of different polysilicon films measured from three 10 μm ×10 μm surfaces with an AFM.

Polysilicon	RMS roughness (nm)	Avg. mean to valley (nm)	Mean to peak valley (nm)
Undoped laminated	9.5 ± 0.7	17.1 ± 1.0	22.2 ± 2.2
0.5% PSG laminated	8.1 ± 0.3	16.7 ± 0.8	23.4 ± 0.3
2% PSG laminated	8.0 ± 0.3	17.4 ± 0.6	24.7 ± 1.5
Undoped columnar	7.8 ± 0.7	18.3 ± 0.3	28.8 ± 1.1
0.5% PSG columnar	8.5 ± 0.6	18.3 ± 0.9	29.0 ± 2.1
2% PSG columnar	8.6 ± 0.7	21.2 ± 1.1	37.7 ± 5.1

Table 5. Comparison of experimentally measured strength of polysilicon specimens with as-deposited sidewalls and ion milled sidewalls using FIB with that predicted using a semi-elliptical crack as the flaw geometry.

Polysilicon	Flaw Geometry		$\sigma_{f,Predicted}$	$\sigma_{f,as\text{-}is}$	$\sigma_{f,FIB}$
	a **(nm)**	***2c*** **(nm)**	**(GPa)**	**(GPa)**	**(GPa)**
Undoped laminated	25	500	2.7	2.3±0.2	2.2±0.2
0.5% PSG laminated	25	500	2.7	-	-
2% PSG laminated	25	500	2.7	2.5±0.2	2.2±0.1
Undoped columnar	30	1200	2.4	1.3±0.1	2.3±0.2
0.5% PSG columnar	30	1200	2.4	1.3±0.1	2.2±0.2
2% PSG columnar	40	1200	2.1	0.95±0.1	1.9±0.1

Table 6. Comparison of experimentally measured strength of polysilicon specimens with as-deposited sidewalls with that predicted using a quarter elliptical edge crack as the flaw geometry.

Polysilicon	Flaw Geometry		$\sigma_{f,Predicted}$	$\sigma_{f,as\text{-}is}$
	a **(nm)**	***c*** **(nm)**	**(GPa)**	**(GPa)**
Undoped laminated	25	500	2.6	2.3±0.2
0.5% PSG laminated	25	500	2.6	-
2% PSG laminated	25	500	2.6	2.5±0.2
Undoped columnar	100	500	1.35	1.3±0.1
0.5% PSG columnar	100	500	1.35	1.3±0.1
2% PSG columnar	500	500	0.85	0.95±0.1

[1] http://mems.sandia.gov/gallery/images.html

[2] A. McCarty, I. Chasiotis, “Description of brittle failure of non-uniform MEMS geometries”, *Thin Solid Films*, vol. 515, pp. 3267-3276, 2007

[3] I. Chasiotis, W.G. Knauss, "The mechanical strength of polysilicon films: Part 2. Size effects associated with elliptical and circular perforation", *J. Mechanics and Phys. Solids*, vol. 51, no. 8, pp. 1551-15, 2003

[4] D.C. Miller, B.L. Boyce, P.G. Kotula, C.R. Stoldt, "Connections between morphological and mechanical evolution during galvanic corrosion of micromachined polycrystalline and monocrystalline silicon", *J. Appl. Phys.*, vol. 103, 123518, 2008.

[5] T. Alan, M.A. Hines, A.T. Zehnder, "Effect of surface morphology on the fracture strength of silicon nanobeams", *Appl. Phys. Lett.*, vol. 89, no. 9, Art. no. 091901, 2006

[6] W. Sharpe Jr., K. Jackson, J. Hemker, Z. Xie, "Effect of specimen size on young's modulus and fracture strength of polysilicon", *J. Microelectromech. Syst.,* vol. 10, no. 3, pp. 317-326, 2001

[7] J. Koskinen, J. Steinwall, R. Soave, H. Johnson, "Microtensile testing of free-standing polysilicon fibers of various grain sizes", *J. Micromech. Microeng.*, vol. 3, no. 1, pp. 13-17, 1993

[8] B.L. Boyce, J.M. Grazier, T.E. Buchheit and M.J. Shaw, "Strength distributions in polycrystalline silicon MEMS", *J. Microelectromech. Syst.*, vol. 16, no. 2, pp. 179-190, 2007

[9] S.S. Hazra, M.S. Baker, J.L. Beuth, M.P. De Boer, "Demonstration of an in situ on-chip tensile tester", *J. Micromech. Microeng.*, vol. 19, no. 8, art. no. 082001, 2009

[10] E.D. Reedy Jr., B.L. Boyce, J.W. Foulk III, R.V. Field Jr.,M.P. de Boer, and S.S. Hazra, "Predicting fracture in micrometer-scale polycrystalline silicon MEMS structures", *J. Microelectromech. Syst.*, vol. 20, no. 4, pp.922-932, 2011

[11] W. Sharpe Jr, K. Jackson, K. Hemker, and Z. Xi, " Effect of specimen size on Young’s modulus and fracture strength of polysilicon", *J. Microelectromech. Syst*., vol. 10, pp. 317-326, 2001

[12] I. Chasiotis, “Mechanics of thin films and microdevices”, IEEE Trans. Device Mater. Rel., vol. 4, no. 2, pp. 176-188, 2004

[13] I. Chasiotis, W.G. Knauss, “The mechanical strength of polysilicon films: Part 1. The influence of fabrication governed surface conditions”, *J. Mechanics and Phys. Solids*, vol. 51, pp. 1533-1550, 2003

[14] H. Kahn, C. Deeb, I. Chasiotis, and A.H. Heuer, “Anodic oxidation during MEMS processing of silicon and polysilicon: native oxides can be thicker than you think”, *J. Microelectromech. Syst*., vol 14, no. 5, pp. 914-923, 2005

[15] R. Ballarini, H. Kahn, N. Tayebi, and A.H. Heuer, "Effects of microstructure on the strength and fracture toughness of polysilicon: A wafer level testing approach," *ASTM special tech. pub*., vol. 1413, pp. 37-51, 2001

[16] T. Tsuchiya, J. Sakata and Y. Taga, "Tensile strength and fracture toughness of surface micromachined polycrystalline silicon thin films prepared under various conditions" *MRS Symp. Proc.*, vol. 505 , pp. 285-290, 1997

[17] T. Kammins, "Structure”, in *Polycrystalline silicon for integrated circuits and displays*, 2nd ed., Kluwer Acadamic Publishers, pp. 103-114

[18] F. Ebrahimi, and L. Kalwani, "Fracture anisotropy in silicon single crystal", *Mater. Sci. Eng. A*, vol. 268, no. 1-2, pp. 116-126, 1999

[19] C.P. Chen, and M.H. Leipold, "Fracture toughness of silicon", *Amer. Cer. Soc. Bulletin*, vol. 59, pp. 519, 1980

[20] Y. Tsai and J. Mecholsky, "Fractal fracture of single crystal silicon", *J. Mater. Resources*, vol. 6, pp. 1248–1263, 1991

[21] A.M. Fitzgerald, R.H. Dauskardt and T.W. Kenny, "Fracture toughness and crack growth phenomena of plasma-etched single crystal silicon", *Sens. and Actuat. A*, 83, pp. 194–199, 2000

[22] H. Kahn, N. Tayebi, R. Ballarini, R.L. Mullen, and A.H. Heuer, "Fracture toughness of polysilicon MEMS devices", *Sens. Actuat. A: Phys.*, vol. 82, no. 1-3, pp. 274-280, 2000

[23] J. Bagdahn, J. Schischka, M. Petzold, and W.N. Sharpe Jr., "Fracture toughness and fatigue investigations of polycrystalline silicon", *Proc. of SPIE - The Inter. Soc. Opt. Eng.,* vol. 4558, pp. 159-168, 2001

[24] I. Chasiotis, S.W. Cho, and K. Jonnalagadda, "Fracture toughness and subcritical crack growth in polycrystalline silicon", *J. Appl. Mech.*, vol. 73, no. 5, pp. 714-722, 2006

[25] S.W. Cho, K. Jonnalagadda, and I. Chasiotis, "Mode I and mixed mode fracture of polysilicon for MEMS", *Fatigue and Fracture of Eng. Mater. Struct.*, vol. 30, no. 1, pp. 21-31, 2007

[26] J.W. Foulk, III, G.C. Johnson, P.A. Klein, and R.O. Ritchie, "A micromechanical basis for partitioning the evolution of grain bridging in brittle materials", *J. Mech. Phys. Solids*, vol. 55, no. 4, pp. 719-743, 2007

[27] J.W. Foulk, III, G.C. Johnson, P.A. Klein, and R.O. Ritchie, "On the toughening of brittle materials by grain bridging: Promoting intergranular fracture through grain angle, strength, and toughness", *J. Mech. Phys. Solids*, vol. 56, no. 6, pp. 2381-2400, 2008

[28] Z. Zeng, X. Ma, J. Chen, Y. Zeng, D. Yang, and Y. Liu, "Effects of heavy phosphorus-doping on mechanical properties of Czochralski silicon", *J. Appl. Phys.*, vol. 107, no. 12, pp. 123503-1-5, 2010

[29] J. G. Swadener and M. Nastasi, "Effect of dopants on the fracture toughness of silicon", *J. Mater. Sci. Lett.*, vol. 21, no. 17, pp. 1363-1365, 2002

[30] K. Park, S. Batra and S. Banerjee, "Role of negatively charged vacancies in secondary grain growth in polycrystalline silicon during rapid thermal annealing", *Appl. Phys. Lett.*, vol. 58, pp. 2414-2416, 1991

[31] V.P. Lesnikova, A.S. Turtsevich, V.Y. Krasnitsky, V.A. Emelyanov, O.Y. Nalivaiko, S.V. Kravtsov and T.V. Makarevich, "The structure, morphology and resistivity of in situ phosphorus doped polysilicon films", *Thin Solid Films*, vol. 247, pp. 156-161, 1994

[32] R. Plugaru, E. Vasile, C. Cobianu and D. Dascalu, "Investigation of the surface of P-implated LPCVD silicon films", Mater. Sci. Eng. B, vol. 42, pp. 240-242, 1996

[33] B.L. Boyce, M.J. Shaw, P. Lu, and M.T. Dugger, "Stronger silicon for microsystems", *Acta Materialia*, vol. 58, pp. 439–448, 2010

[34] J. J. Sniegowski and M. P. de Boer, "IC-compatible polysilicon surface micromachining", *Annual Rev. Mater. Sci.*, vol. 30, pp. 299-333, 2000

[35] S.W. Cho and I. Chasiotis, “Elastic Properties and Representative Volume Element of Polycrystalline Silicon for MEMS”, *Exper. Mech.*, vol. 47, no. 1, pp. 37-49, 2007

[36] K. Jonnalagadda, I. Chasiotis, S. Yagnamurthy, J. Lambros, J. Pulskamp, R. Polcawich, and M. Dubey, "Experimental investigation of strain rate dependence of nanocrystalline Pt films", *Exper. Mech.*, vol. 50, pp. 25-35, 2010

[37] H. Tada, P. C. Paris, and G. R. Irwin, "The stress analysis of cracks handbook", 3rd ed., ASME Press, New York, pp. 52–53, 2000

[38] A. Hallinan Jr., "A review of the Weibull distribution", *J. Quality Tech.*, vol. 25., no. 2, pp. 85-93, 1993

[39] W.M. Robertson, "Thermal etching and grain-boundary grooving of silicon ceramics", *J. Amer. Cer. Soc.*, vol. 64, no. 1, pp. 9-13, 1981

[40] Y. Wada and S. Nishimatsu, "Grain growth mechanism of heavily phosphorus implanted polycrystalline silicon", *J. Electrochem. Soc.*, vol. 125, no. 9, pp. 1499-1504, 1978

[41] M. Steyer, A. Dastgheib-Shirazi, H. Wagner, G. Micard, P.P. Altermatt, and G. Hahn, "A study of various methods for the analysis of the phosphosilicate glass layer", *27th European Photovoltaic Solar Energy Conf. Exhib. in Frankfurt, Germany*, pp. 1325-1328, 2012

[42] D.R. Lide, "Handbook of chemistry and physics", 85th Ed, CRC Press LLC

[43] J.C. Newman and I.S Raju, "Stress intensity factor equations for cracks in three-dimensional finite bodies", ASTM STP791-EB / STP37074S, 1983